Geophysical & Astrophysical Fluid Dynamics

Publication details, including instructions for authors and subscription information:
http://www.tandfonline.com/loi/ggaf20

Baroclinic multipole evolution in shear and strain

Mikhail A. Sokolovskiy [a] , Konstantin V. Koshel [b] & Xavier Carton [c]

[a] Water Problems Institute of RAS, 3, Gubkina Str., 119333, Moscow, Russia

[b] V.I. Il'ichev Pacific Oceanological Institute of FEB RAS, 43 Baltiyskaya Str., 690041, Vladivostok, Russia

[c] Laboratoire de Physique des Océans, UFR Sciences, UBO, 6 Av. Le Gorgeu, 29200 Brest, France

Available online: 13 Jul 2011

To cite this article: Mikhail A. Sokolovskiy, Konstantin V. Koshel & Xavier Carton (2011): Baroclinic multipole evolution in shear and strain, Geophysical & Astrophysical Fluid Dynamics, 105:4-5, 506-535

To link to this article: http://dx.doi.org/10.1080/03091929.2010.533662

Geophysical and Astrophysical Fluid Dynamics
Vol. 105, Nos. 4–5, August–October 2011, 506–535

Baroclinic multipole evolution in shear and strain

MIKHAIL A. SOKOLOVSKIY†*, KONSTANTIN V. KOSHEL‡ and XAVIER CARTON§

†Water Problems Institute of RAS, 3, Gubkina Str., 119333, Moscow, Russia
‡V.I. Il'ichev Pacific Oceanological Institute of FEB RAS, 43 Baltiyskaya Str., 690041, Vladivostok, Russia
§Laboratoire de Physique des Océans, UFR Sciences, UBO, 6 Av. Le Gorgeu, 29200 Brest, France

(*Received 10 December 2009; in final form 28 April 2010; first published online 10 December 2010*)

In a two-layer quasi-geostrophic model, the evolution of a symmetric baroclinic multipole, composed of a central vortex with strength $\mu\kappa$ in the upper layer, and A satellites with strength κ in the lower layer, is studied. This multipole is imbedded in a center-symmetric shear/strain field, either steady or time-periodic. Special attention is given to the case of the tripole ($A=2$). The stability of this tripole is assessed and its oscillations in the external field are analyzed. Conditions for resonance of these oscillations are derived and transition to chaos is described.

Keywords: Vortex multipoles; Tripole; Two-layer quasi-geostrophic model; Chaos; Nonlinear resonances

1. Introduction

Vortices play an essential role in the advection and diffusion of momentum, heat and tracers in planetary fluids and in turbulence strongly constrained by global rotation and ambient stratification (McWilliams 1984). In particular, the strength of vortices versus that of neighboring sheared currents allows them to maintain an identifiable and relatively invariant structure for long times. Experiments and observations have shown that many vortices have a monopolar structure, but not all (Richardson *et al*. 1979, Kennelly *et al*. 1985, Horton and Baylor 1991, Nof 1993, Kennan and Flament 2000, Carton 2001, Baey and Carton 2002). Laboratory experiments and simulations have also shown that, when moderately disturbed, unstable circular vortices would rearrange as multipoles (Smeed 1988, Thivolle-Cazat *et al*. 2005). The simplest multipoles (dipoles and tripoles in a 2D incompressible fluid) were shown to be also long-lived (McWilliams 1984, Sutyrin 1994). Other studies evidenced that multipolar vortices can also form and live for long durations in stratified rotating fluids (Morel and Carton 1994, Corréard and Carton 1999).

*Corresponding author. Email: sokol@aqua.laser.ru

Geophysical and Astrophysical Fluid Dynamics
ISSN 0309-1929 print/ISSN 1029-0419 online
DOI: 10.1080/03091929.2010.533662

The heton (an association of a cyclonic and an anticyclonic eddy at different depths) has been intensively studied (Gryanik 1983, Hogg and Stommel 1985a, b, Kizner 2006, Gryanik *et al*. 2006). Its stability and mutual interactions have been quantified. In particular, nearly elastic collisions can occur (Sokolovskiy and Verron 2000, Gryanik *et al*. 2006). Heton collisions (like baroclinic vortex instability) can give birth to baroclinic multipoles. The stability or evolution of such baroclinic multipoles, either isolated or in the presence of other vortices or currents, has not yet been extensively studied, and is a subject of interest for turbulence or planetary fluid motions. In particular, tripolar baroclinic structures (such as omega blocks) are present in the Earth atmosphere (Davis *et al*. 1993). Baroclinic quadrupoles have been shown to form from the instability of the loop current (Chérubin *et al*. 2006). These vortices are always imbedded in larger scale currents or winds.

The purpose of this study is to investigate the stability and evolution of a generic baroclinic tripole to surrounding shear and strain flow. In that respect, we first analyze the motion of a tripolar point vortex aggregate in a center-symmetric shear/strain field, firstly steady and then time-periodic. Then, the stability and chaotic evolutions of these tripoles is analyzed via multiple time expansion. Transition to chaos is evidenced, and the evolution of separatrices and homoclinic curves are described with Poincaré maps. Consequences are drawn for geophysical vortices.

2. Mathematical and physical framework

Under strong influence of ambient rotation and stratification (small Rossby number and order unity Burger number), incompressible fluid flows are governed by the quasi-geostrophic equations. In a two-layer configuration, in the absence of dissipation, and in the presence of the external field

$$\Psi = -\frac{1}{2}\left[S(t)\left(x^2 - y^2\right) - \Omega(t)\left(x^2 + y^2\right)\right], \tag{1}$$

these equations express the conservation of potential vorticity:

$$\partial_t q_j + J(\psi_j, q_j) = 0 \tag{2}$$

with

$$q_j = \nabla^2 \psi_j + F_j(\psi_{3-j} - \psi_j) + f_0 + 2\Omega$$

the potential vorticity in layer $j = 1, 2$ (upper, lower). The stream function in layer j is ψ_j and f_0 is the Coriolis parameter. The layer coupling coefficients are $F_j = f_0^2/(g' H_j)$, where g' is the reduced gravity and H_j is the thickness of layer j at rest. The internal radius of deformation is

$$R_d = \sqrt{g' h_1 h_2 (h_1 + h_2)^{-1}} \Big/ f_0 = 1/\gamma$$

and the vertical (barotropic and baroclinic) modes are defined by

$$\psi_{bt} = h_1 \psi_1 + h_2 \psi_2, \quad \psi_{bc} = \psi_1 - \psi_2$$

with $h_j = H_j/H$ ($H = H_1 + H_2$). With these definitions, we have

$$q_{bt} = \nabla^2 \psi_{bt} + 2\Omega, \quad q_{bc} = \nabla^2 \psi_{bc} - \gamma^2 \psi_{bc}.$$

Note that S and Ω are the strain and rotation components of the external field: if they are positive, stretching occurs along the $y = -x$ direction (resp. contraction occurs along $y = x$) and cyclonic rotation around the origin of the (x, y) plane; if they are negative, all directions are reversed. An external flow of form (1) has a critical point (0; 0) of elliptic type when $|\Omega| > |S|$ and of hyperbolic type when $|\Omega| \le |S|$.† For oceanic application, a nearly barotropic shear can correspond to the Antarctic circumpolar current in which hetons have been observed (Savchenko *et al.* 1978).

Labeling vortex coordinates (x_j^α, y_j^α) with j as the layer index ($j = 1, 2$) and α as the vortex number in layer j ($\alpha = 1, 2, \ldots, A_j$). Point vortex motion obeys the following equations:

$$\dot{x}_j^\alpha = -(S+\Omega) y_j^\alpha - \frac{h_j}{2\pi} \left\{ \sum_{\substack{\beta=1 \\ \beta \neq \alpha}}^{A_j} \kappa_j^\beta \frac{y_j^\alpha - y_j^\beta}{(r_{jj}^{\alpha\beta})^2} \left[1 + \frac{h_{3-j}}{h_j} \gamma r_{jj}^{\alpha\beta} \mathrm{K}_1\left(\gamma r_{jj}^{\alpha\beta}\right) \right] \right.$$
$$\left. + \sum_{\beta=1}^{A_{3-j}} \kappa_{3-j}^\beta \frac{h_{3-j}}{h_j} \frac{y_j^\alpha - y_{3-j}^\beta}{\left(r_{j(3-j)}^{\alpha\beta}\right)^2} \left[1 - \gamma r_{j(3-j)}^{\alpha\beta} \mathrm{K}_1\left(\gamma r_{j(3-j)}^{\alpha\beta}\right) \right] \right\}, \tag{3}$$

$$\dot{y}_j^\alpha = -\left(S-\Omega\right) x_j^\alpha + \frac{h_j}{2\pi} \left\{ \sum_{\substack{\beta=1 \\ \beta \neq \alpha}}^{A_j} \kappa_j^\beta \frac{x_j^\alpha - x_j^\beta}{\left(r_{jj}^{\alpha\beta}\right)^2} \left[1 + \frac{h_{3-j}}{h_j} \gamma r_{jj}^{\alpha\beta} \mathrm{K}_1\left(\gamma r_{jj}^{\alpha\beta}\right) \right] \right.$$
$$\left. + \sum_{\beta=1}^{A_{3-j}} \kappa_{3-j}^\beta \frac{h_{3-j}}{h_j} \frac{x_j^\alpha - x_{3-j}^\beta}{\left(r_{j(3-j)}^{\alpha\beta}\right)^2} \left[1 - \gamma r_{j(3-j)}^{\alpha\beta} \mathrm{K}_1\left(\gamma r_{j(3-j)}^{\alpha\beta}\right) \right] \right\}, \tag{4}$$

where, $r_{ij}^{\alpha\beta} = \sqrt{(x_i^\alpha - x_j^\beta)^2 + (y_i^\alpha - y_j^\beta)^2}$ is the distance between vortex β in the j-th layer and vortex α in the i-th layer, κ_j^β is the strength of the vortex with the same indices and K_1 is modified Bessel function of order 1.

Let us further assume that $h_1 = h_2 = 1/2$, $A_1 = 1$, $A_2 = A$, $\kappa_1^1 = \mu\kappa$, $\kappa_2^1 = \kappa_2^2 = \cdots = \kappa_2^A = \kappa$, and that the two-layer vortex configuration with a central vortex in the upper layer has A-fold symmetry:

$$x_1^1 = y_1^1 = 0, \tag{5}$$

$$\left(x_2^\alpha;\ y_2^\alpha\right) = \rho \left\{ \cos\left[\theta + \frac{2\pi(\alpha-1)}{A}\right]; \sin\left[\theta + \frac{2\pi(\alpha-1)}{A}\right] \right\}. \tag{6}$$

We note that linear and angular momenta are conserved, and we insert the vortex coordinates (5), (6) ($\rho = \rho(t)$, $\theta = \theta(t)$), into the equations of motion (3), (4). We obtain

$$\dot{\rho} = -\frac{\kappa}{4\pi} s \rho \sin\left[2\left(\theta + \frac{2\pi(\alpha-1)}{A}\right)\right], \tag{7}$$

†Both types of critical points are known to be present, in particular, in stationary planetary waves, e.g. Hartman (1977).

$$\dot{\theta} = \frac{\kappa}{4\pi}\left\{\frac{1}{\rho^2}\left[\frac{A-1}{2} + \mu\left[1 - \gamma\rho \mathrm{K}_1(\gamma\rho)\right] + \gamma\rho\sum_{\beta=1}^{A-1}\sin\frac{\pi\beta}{A}\mathrm{K}_1\left(2\gamma\rho\sin\frac{\pi\beta}{A}\right)\right]\right.$$
$$\left. + \omega - s\cos\left[2\left(\theta + \frac{2\pi(\alpha-1)}{A}\right)\right]\right\}, \tag{8}$$

where $s(t) = 4\pi S(t)/\kappa$, $\omega(t) = 4\pi\Omega(t)/\kappa$ and $\alpha = 1, 2, \ldots, A$ in (5)–(8).

3. Equilibria and stability

Following Kawakami and Funakoshi (1999), the Jacobian matrix of (7)–(8) has the form

$$J = \frac{\kappa}{4\pi}\begin{pmatrix} J_{11} & J_{12} \\ J_{21} & J_{22} \end{pmatrix}, \tag{9}$$

where

$$J_{11} = -s\sin\left[2\left(\theta + \frac{2\pi(\alpha-1)}{A}\right)\right],$$
$$J_{12} = 2s\rho\cos\left[2\left(\theta + \frac{2\pi(\alpha-1)}{A}\right)\right],$$
$$J_{21} = -\frac{2}{\rho^3}\left[\frac{A-1}{2} + \mu\left[1 - \gamma\rho\mathrm{K}_1(\gamma\rho)\right] + \gamma\rho\sum_{\beta=1}^{A-1}\sin\frac{\pi\beta}{A}\mathrm{K}_1\left(2\gamma\rho\sin\frac{\pi\beta}{A}\right)\right] \tag{10}$$
$$+\frac{\gamma^2}{\rho}\left[\mu\mathrm{K}_0(\gamma\rho) - 2\sum_{\beta=1}^{A-1}\sin^2\frac{\pi\beta}{A}\mathrm{K}_0\left(2\gamma\rho\sin\frac{\pi\beta}{A}\right)\right],$$
$$J_{22} = 2s\sin\left[2\left(\theta + \frac{2\pi(\alpha-1)}{A}\right)\right].$$

When $\dot{\rho} = \dot{\theta} = 0$ and $\omega = \omega_0$, $s = s_0$ are constant, the positions of the stationary points are defined by polar angles

$$\theta = \theta_0(A, \alpha, n) = \pi\left[\frac{n-1}{2} - \frac{2(\alpha-1)}{A}\right] \tag{11}$$

and radii $\rho = \rho_0(A, n, \mu, \omega_0, s_0)$ such as

$$\frac{1}{\rho_0^2}\left[\frac{A-1}{2} + \mu\left[1 - \gamma\rho_0\mathrm{K}_1(\gamma\rho_0)\right] + \gamma\rho_0\sum_{\beta=1}^{A-1}\sin\frac{\pi\beta}{A}\mathrm{K}_1\left(2\gamma\rho_0\sin\frac{\pi\beta}{A}\right)\right] + \omega_0 + (-1)^n s_0 = 0, \tag{12}$$

where $n = 1, 2$ and $\alpha = 1, 2, \ldots, A$.

In this case, Jacobian (9) takes a simpler form

$$J^{(0)} = \frac{\kappa}{4\pi}\begin{pmatrix} J_{11}^{(0)} & J_{12}^{(0)} \\ J_{21}^{(0)} & J_{22}^{(0)} \end{pmatrix}, \tag{13}$$

where

$$J_{11}^{(0)} = J_{22}^{(0)} = 0, \quad J_{12}^{(0)} = 2s_0\rho_0(-1)^{n-1},$$

$$J_{21}^{(0)} = \frac{1}{\rho_0}\left\{2\big(\omega_0 + s_0(-1)^n\big) + \gamma^2\left[\mu \mathrm{K}_0(\gamma\rho_0) - 2\sum_{\beta=1}^{A-1}\sin^2\frac{\pi\beta}{A}\mathrm{K}_0\left(2\gamma\rho_0\sin\frac{\pi\beta}{A}\right)\right]\right\}. \qquad (14)$$

The solution of equations (11), (12), if it exists, given the external parameters, determines the stationary position (ρ_0, θ_0) of the lower layer vortices.

The particular case ($\omega_0 = s_0 = 0$) of the stationary problem was considered in the study by Sokolovskiy and Verron (2006); they showed that for any A, there exists a critical value $\mu_{\mathrm{cr}} < 0$, such that an appropriate solution exists whatever $\mu \le \mu_{\mathrm{cr}}$. The steady motion of the multipolar structure is a cyclonic rotation for $\rho < \rho_0$ (a motion called *inverse roundabout* for which intralayer interaction is dominant); for $\rho = \rho_0$, steady states are found. For $\rho > \rho_0$, anticyclonic rotation of the vortices occurs under the influence of the central vortex of the upper layer (this is an *ordinary roundabout*).

The addition of cyclonic/anticyclonic external rotation ω_0 increases/reduces ρ_0 (in the absence of external strain). With external strain (s_0), and assuming a positive ω_0, the situation changes qualitatively as can be seen from figure 1, where solutions of equation (12) are plotted. The curves in the (ρ, Δ) plane represent the steady-state solutions for multipoles for different values of A and of μ. Here Δ denotes one of values $\Delta_{\mp} = \omega_0 \mp s_0$, and distance ρ is calculated along the radial axis at angle θ_0 in (11). Clearly, the particular case $\omega_0 = s_0 = 0$ mentioned above corresponds to the intersection points of the curves with the ρ-axis.

As can be seen from the figure, when μ is nonpositive, all curves are nonmonotonic and attain a maximum at some value $\Delta = \Delta_{\max}$. Since the opposite polarity of the central vortex in the upper layer can be one of the causes for the existence of stationary positions of vortices in the lower layer, it is clear that an increase in the number of vortices in the lower layer at fixed μ results in a decrease in $\Delta_{\max}$. Indeed, with the addition of satellite vortices, their collective cyclonic rotation increases, preventing a possible steady state. A similar trend can be seen with a decline in the core strength (figures 1(a) and (b)). Now we will consider the particular case of a tripole $A = 2$. In this

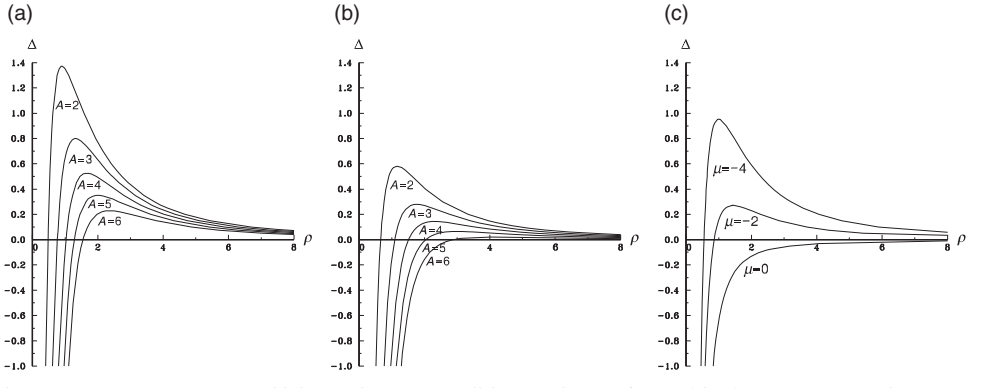

Figure 1. Curves $\Delta(\rho)$, on which steady-state condition (3) is met for multipoles: (a) $\mu = -5$, (b) $\mu = -3$ for the specified values of A, and (c) $A = 2$ for the indicated values of μ.

case (11), (12) and the expression for $J_{21}^{(0)}$ in (14) becomes simpler and yields

$$\theta = \theta_0(\alpha, n) = \pi\left(\frac{n+1}{2} - \alpha\right), \quad n, \alpha = 1, 2, \tag{15}$$

$$\frac{1}{\rho_0^2}\left[\frac{1}{2} + \mu\left[1 - \gamma\rho_0 \mathrm{K}_1(\gamma\rho_0)\right] + \gamma\rho_0 \mathrm{K}_1(2\gamma\rho_0)\right] + \omega_0 + (-1)^n s_0 = 0, \tag{16}$$

$$J_{21}^{(0)} = \frac{1}{\rho_0}\left[2\left(\omega_0 + s_0(-1)^n\right) + \gamma^2\left[\mu \mathrm{K}_0(\gamma\rho_0) - 2\mathrm{K}_0(2\gamma\rho_0)\right]\right]. \tag{17}$$

The eigenvalues of matrix (13) can be determined from

$$\lambda_{1,2} = \pm\sqrt{J_{12}^{(0)} J_{21}^{(0)}}. \tag{18}$$

Whence it follows that, if equation (16) has solutions for both $n = 1$ and $n = 2$, then, in view of the alternating sign of $J_{12}^{(0)}$ (see (14)), two solutions are always stable, and two are unstable.

Returning to figure 1, we note that when both values Δ_- and Δ_+ are larger than $\Delta_{\max}$, there are no stationary positions. However, if at least one of those values is smaller than $\Delta_{\max}$, then, at $A = 2$, cases with one, two, three, or four pairs of stationary points are possible. In the latter case, the condition

$$0 < \Delta_-, \Delta_+ \leq \Delta_{\max} \tag{19}$$

should be met.

Below, we will consider an even narrower class of vortex structures with zero total strength: $A = 2$ and $\mu = -2$.

In figure 1, this case corresponds to the median curve of panel (c), where $\Delta_{\max} \equiv \Delta_{\max}|_{\mu=-2}^{A=2} = 0.27094$. As can be seen from solution (15)–(16), stationary points always lie on the x- and y-axes. The value Δ_- corresponds to stationary points on the x-axis; note that hyperbolic singularities always lie on the left branch of the curve and elliptic points, on its right branch. Again Δ_+ characterizes singularities along the y-axis, where elliptic singularities lie on the left branch of the curve, and hyperbolic singularities, on its right branch.

Figure 2 gives four cases of vortex trajectories for the lower layer (the vortex in the upper layer is fixed at the origin) for external parameters for which four pairs of singularities always exist. External field parameters (ω_0, s_0) and the coordinates of the singular points for each case are given in the caption. Those examples vividly demonstrate the role of rotation and strain components of the external field (1) in the dynamics of the lower layer. A common feature of those figures is the presence of two separatrices (an internal and an external) both having similar character and being either heteroclinic or homoclinic. Their topological features depend on which class the vortex structure belongs to. First of all we note that an element in common with the free-tripole problem is the presence of *inverse roundabouts* in the central domain, where two satellite vortices rotate in the cyclonic direction along a common trajectory. The rotation in the external domain (beyond both separatrices) in all such cases is also cyclonic, since ω_0 (>0) plays a key role here.

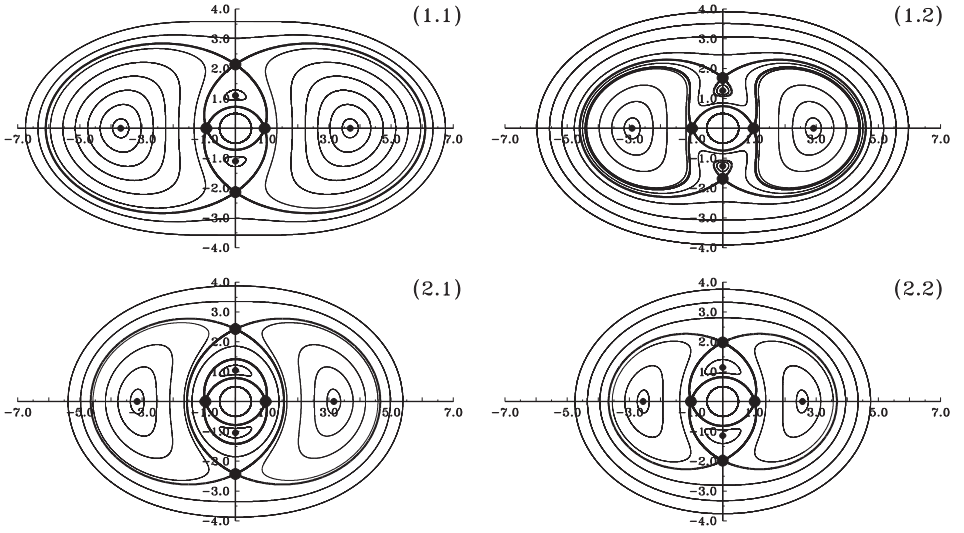

Figure 2. Gallery of vortex trajectories in the lower layer, which correspond to the four small black circle markers in figure 3. (**1.1**): $\omega_0 = 0.1574$, $s_0 = 0.0569$; $\rho_{1,h} = (\pm 0.9377; 0)$, $\rho_{1,e} = (\pm 3.6893;\ 0)$, $\rho_{2,e} = (0; \pm 1.0989)$, $\rho_{2,h} = (0; \pm 2.1412)$;(**1.2**): $\omega_0 = 0.2024$,$s_0 = 0.0569$; $\rho_{1,h} = (\pm 0.9862; 0)$, $\rho_{1,e} = (\pm 2.9151;\ 0)$, $\rho_{2,e} = (0; \pm 1.2612)$, $\rho_{2,h} = (0; \pm 1.6849)$; (**2.1**): $\omega_0 = 0.1574$, $s_0 = 0.0284$; $\rho_{1,h} = (\pm 0.9664; 0)$, $\rho_{1,e} = (\pm 3.1595;\ 0)$, $\rho_{2,e} = (0; \pm 1.0436)$, $\rho_{2,h} = (0; \pm 2.4296)$; (**2.2**): $\omega_0 = 0.2024$, $s_0 = 0.0284$; $\rho_{1,h} = (\pm 1.0249; 0)$, $\rho_{1,e} = (\pm 2.5598;\ 0)$, $\rho_{2,e} = (0; \pm 1.1413)$, $\rho_{2,h} = (0; \pm 1.9821)$. (Here, the values of $n = 1$, 2 correspond to the first subscripts of variable ρ, while the denotations "e" and "h" refer to the coordinates of elliptic and hyperbolic stationary points, respectively). The thick lines show separatrices separating domains with different types of motion. The diagonal fragments (1.1), (2.2) represent the cases of reconnections. Here, the motions in the central, lateral, and external domains are cyclonic, while those in the lunate domains are anticyclonic.

Let us consider the major features of those motions:

- Two classes of different motions can be identified: *S* (similar) and *D* (dissimilar). The appropriate trajectories are shown in the panels below and above the main diagonal, respectively.
- The comparison of images for those two cases shows:

  (1) In case *S*, the external and internal separatrices are topologically similar (though one of them is rotated by 90° with respect to the other); this accounts for the name *S* for this class of motions. In this case, the separatrices consist of two closed domains tangent in two hyperbolic points, i.e. they are heteroclinic structures. In the lateral domains with fixed elliptic points on the *x*-axis (within the external separatrix), vortices move along their own trajectory in the cyclonic direction. Within the internal separatrix, vortices rotate in the anticyclonic direction within lunate domains (along individual trajectories) and within the domain between separatrices (along a common trajectory). In the central domain, their motion has a cyclic character, i.e. is an inverse roundabout.

  (2) In case *D*, two different types of homoclinic separatrices exist, one of which passes through two hyperbolic points on the *y*-axis; a loop corresponds to each of those points. The whiskers that issue from the saddle points merge and pass around four vortex domains: two domains with centers on

the y-axis, belonging to the same homoclinic structure (with anticyclonic motion of vortices), and two domains with centers on the x-axis (with cyclonic vortex motion), which belong to the internal homoclinic structure. The internal separatrix passes through two hyperbolic singular points on the x-axis, and consists of two homoclinic loops, while the whiskers of the saddle points pass around the central domain; this can also be regarded as a heteroclinic structure in combination with the lateral loops of the internal separatrix. An intermediate flow-through domain forms in this case, in the narrow zone between the separatrices; the lower layer vortices in this intermediate domain move along a common trajectory in the anticyclonic direction. The topological difference between the separatrices in this case is that the homoclinic loops lie within the separatrix whiskers for the external separatrix and beyond the domain embraced by the whiskers for the internal separatrix.

(3) Thus, the main differences between those cases are as follows:

(a) The internal separatrix in case S embraces the central domain with cyclonic rotation and vertical lunate domains with anticyclonic motion of vortices, thus forming a heteroclinic structure (the hyperbolic points have no whiskers), while in the case D the central domain is embraced by whiskers consisting of saddle points of the internal separatrix, and they along with the lateral loops issued from saddle points of the homoclinic structure (the right and the left ones) pass around the trajectories of vortices rotating in the cyclonic direction.

(b) The external separatrix in case S consists of two heteroclinic loops located on the x-axis, while in case D, the whiskers of the saddle points of the external separatrix embrace the entire central part of the phase picture, including the homoclinic loops of this separatrix, which now are located on the y-axis;

(c) The anticyclonic flow-through motion involves the central, upper, and lower domains in case S and the central and lateral domains in case D.

- When the conditions $\Delta_- < \Delta_{\max}$ and $\Delta_+ > \Delta_{\max}$ are met simultaneously, for any ω_0 there exist pairs of parameters $\pm s_0^{\text{rec}}$, such that the external and internal separatrices merge to form the so-called reconnection of separatrices and thus the flow-through domains disappear – see panels (1.1) and (2.2) of figure 2. The conditions for a reconnection to appear have the form:

$$F(a) + a^2\Delta_- = F(b) + b^2\Delta_+, \tag{20}$$

where $F(z) = 2\mu F_1(z) + F_2(2z)$ and $F_1(z) = \ln z + \mathrm{K}_0(z)$, $F_2(z) = \ln z - \mathrm{K}_0(z)$; a and b are solutions of equations (15)–(16) for $n = 1$ and for $n = 2$, respectively. Equation (20) represents the requirement that the values of the Hamiltonian are the same on two separatrices passing simultaneously through hyperbolic points on the x- and y-axis.

- When the vortex structure belongs to class S, an increase in both ω_0 and s_0 is accompanied by an increase in the vertical size of lunate domains up to its limit (when its point most distant from the center and lying on the y-axis merges with the hyperbolic singular point, i.e. reconnection takes place). Then the

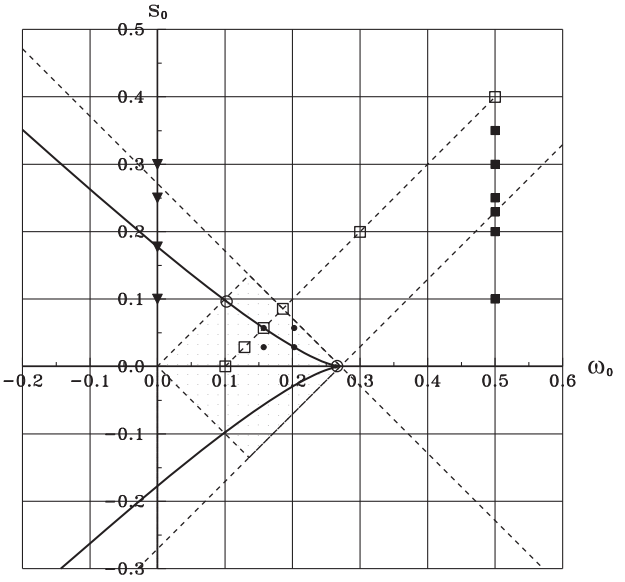

Figure 3. State diagram for a tripole in a steady external field in the (ω_0, s_0) parameter plane at $\mu = -2$. The dashed lines which cross the horizontal axis satisfy the conditions $\Delta_{\mp} = \Delta_{\max}$, the marked-out domain contains the points in the plane where condition (19) is satisfied. The conditions for a reconnection, when separatrices merge, are satisfied on solid lines. The tilted dashed segment passes through markers corresponding to the parameters of experiments in figure 5.

separatrices surrounding it split at the hyperbolic points on the x-axis, these domains become loop-like, and passage to class D takes place. Thus, the passage via reconnection is accompanied by a change in the separatrix type from heteroclinic (S) to homoclinic (D). The opposite transformation takes place in the structures of class D with a decrease in parameters ω_0 and s_0.

Figure 3 gives a state diagram of a tripole in the (ω_0, s_0) plane. The reconnection condition (20) is satisfied on the solid lines. The dashed lines which cross the horizontal axis satisfy the equations $\Delta_- = \omega_0 - s_0 = \Delta_{\max}$ and $\Delta_+ = \omega_0 + s_0 = \Delta_{\max}$. The domain marked out by the dotted line contains the points of the (ω_0, s_0) plane at which condition (19) is met, implying the existence of four pairs of singular points. In this case, $\Delta_{\max} \equiv \Delta_{\max}|_{\mu=-2}^{A=2} = 0.27094$. The positions of markers correspond to the parameters (ω_0, s_0), for which numerical experiments shown in figures 2 and 4–7 were carried out. It can be seen, in particular, that all small circular markers (on a diagonal) belong to the reconnection line.

Some features of the behavior of separatrices during reconnection can be seen in the diagonal panels of figure 2 – (1.1) and (2.2): the elliptic and hyperbolic stationary points move closer to each other along both the x- and y-axes during the downward motion along the upper branch of the reconnection line in figure 3 (i.e. when parameters ω_0 and s_0 decrease simultaneously).

In addition to this picture, figure 4 demonstrates the specific features of separatrices in the neighborhood of accumulation points, in the domain marked out in figure 3. Thus, figure 4(a) presents the case $\omega_0 = s_0$, when the straight line $\Delta_- = 0$ crosses the curve of stationary states in figure 1 at a single point, resulting in a single pair of

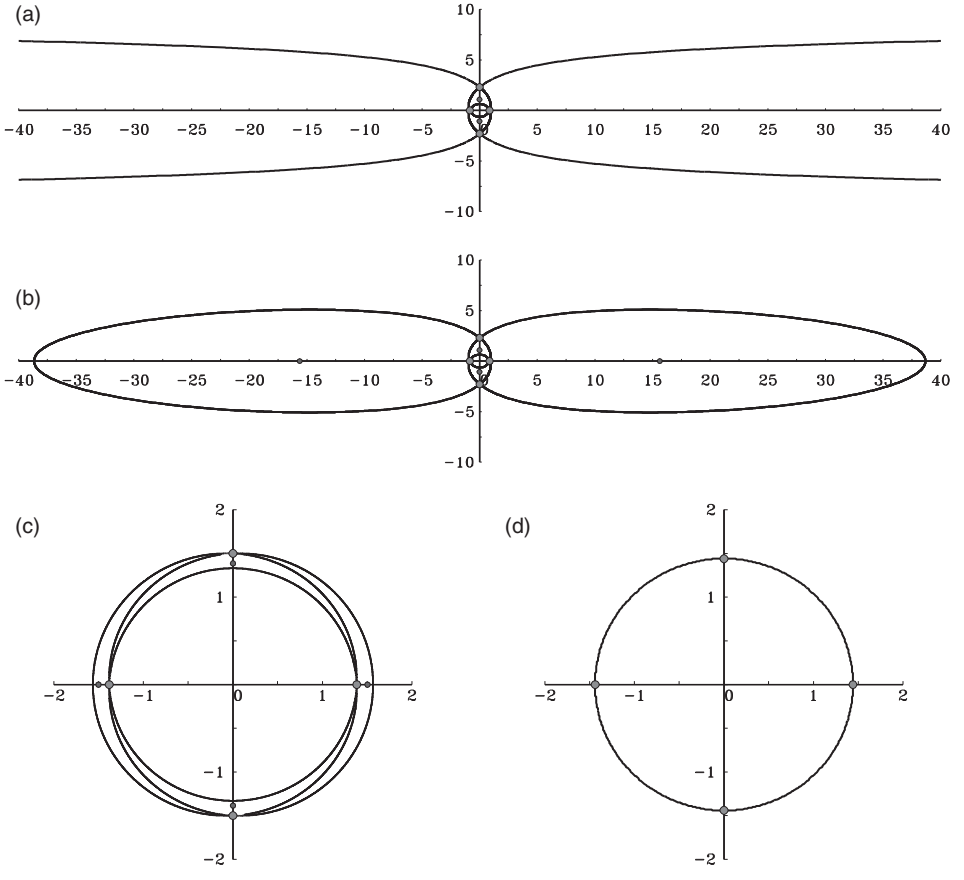

Figure 4. Set of separatrices in the presence of reconnection at accumulation points of the domain marked out in figure 3 and in their neighborhoods: (a) $\omega_0 = s_0 = 0.09889$ ($\Delta_+ = 0.19778$, $\Delta_- = 0$); $\rho_{1h} = (\pm 0.86015;\ 0)$, $\rho_{1e} = (\pm\infty;\ 0)$, $\rho_{2e} = (0;\ \pm 1.06489)$, $\rho_{2h} = (0;\ \pm 2.30437)$; (b) $\omega_0 = 0.10235$, $s_0 = 0.0962$ ($\Delta_+ = 0.19855$, $\Delta_- = 0.00615$); $\rho_{1h} = (\pm 0.86413;\ 0)$, $\rho_{1e} = (\pm 15.61728;\ 0)$, $\rho_{2e} = (0;\ \pm 1.06624)$, $\rho_{2h} = (0;\ \pm 2.29656)$; (c) $\omega_0 = 0.2660$, $s_0 = 0.0006$ ($\Delta_+ = 0.2666$, $\Delta_- = 0.2654$); $\rho_{1h} = (\pm 1.38299;\ 0)$, $\rho_{1e} = (\pm 1.50328;\ 0)$, $\rho_{2e} = (0;\ \pm 1.38591)$, $\rho_{2h} = (0;\ \pm 1.49980)$; (d) $\omega_0 = 0.27094$, $s_0 = 0$ ($\Delta_+ = \Delta_- = 0.27094$); $\rho^* = 1.4407$. Small circles mark the coordinates of elliptical points, and large circles mark the coordinates of hyperbolic points. The respective markers in figure 3 are also represented by circles.

hyperbolic stationary points on the x-axis, while the coordinates of elliptic lateral points tend to their infinite limits. In figure 3, this experiment corresponds to the circle at the intersection of the reconnection line and the rectilinear boundary of the domain under consideration. When Δ_- is positive and small (0.00615 in figure 4(b)), the lateral domains of the closed trajectories with centers at the elliptic points, with coordinates $x_{1e} = \pm 15.6173$, acquire a finite size. In the vicinity of the opposite limit on the reconnection line ($\Delta_+ \sim \Delta_- \sim \Delta_{\max}$ at $s_0 \to 0$), all hyperbolic and elliptic points approach each other in pairs (figure 4(c)) and in the limit $s_0 = 0$, they merge and degenerate (figure 4(d)). It is obvious that the circle with radius $\rho^* = |x_{1e}| = |x_{1h}| = |y_{1e}| = |y_{1h}|$ is the isoline of zero angular rotational velocity of the roundabout. Thus, we have an inverse roundabout both inside and outside this circle. Note that the corresponding markers in figure 3 seem to coincide, since the points in the (ω_0, s_0) plane are very close to each other, for experiments 4(a) and 4(b), as well as for 4(c) and 4(d).

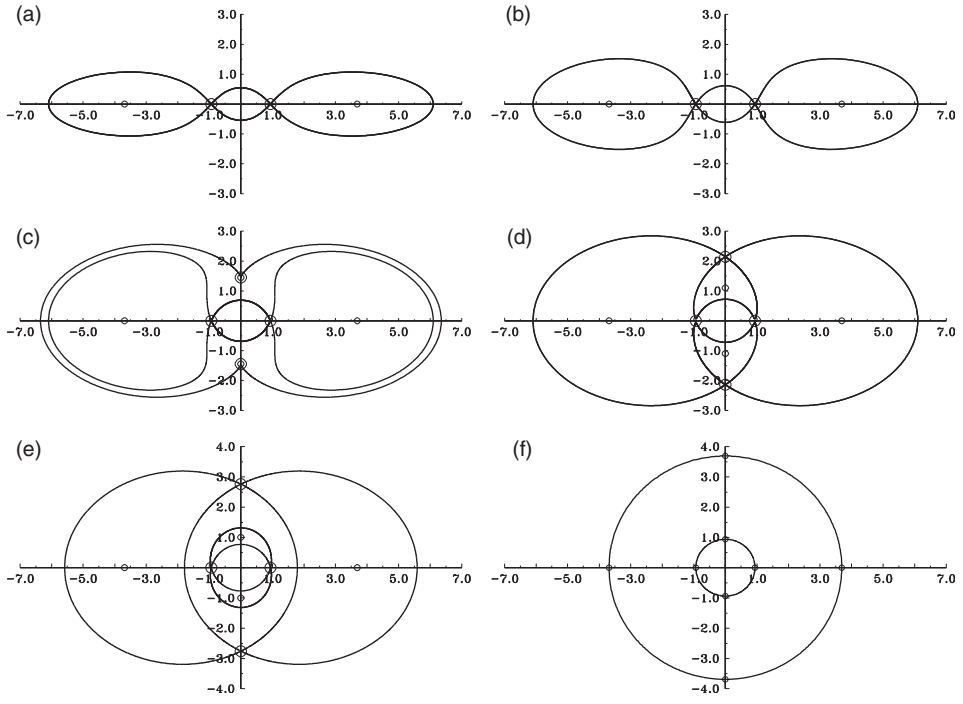

Figure 5. Set of separatrices for the motions of vortices in the lower layer at a fixed value of parameter $\Delta_- = 0.10045$: (a) $\omega_0 = 0.5$, $s_0 = 0.39955$; (b) $\omega_0 = 0.3$, $s_0 = 0.19955$; (c) $\omega_0 = 0.185695$, $s_0 = 0.085240$, $\rho_{2e} = \rho_{2h} = (0;\ \pm 1.44087)$; (d) $\omega_0 = 0.15735$, $s_0 = 0.05690$, $\rho_{2e} = (0;\ \pm 1.09887)$, $\rho_{2h} = (0;\ \pm 2.14116)$; (e) $\omega_0 = 0.12885$, $s_0 = 0.02840$, $\rho_{2e} = (0;\ \pm 1.00123)$, $\rho_{2h} = (0;\ \pm 2.75941)$; (f) $\omega_0 = 0.10045$, $s_0 = 0$, $r_1 = |\rho_{1h}| = 0.93770$, $r_2 = |\rho_{2e}| = 3.68926$ (markers in figure 3 are hollow squares).

Now we examine the topological properties of the separatrices during changes in the external field which preserve the value Δ_-. A series of separatrix configurations for this case is given in figure 5. Figure 3 shows the appropriate hollow-square markers lying on a tilted dashed line determined by equation $\Delta_- = 0.10045$. Under such conditions, the coordinates of stationary points on the x-axis clearly remain unchanged: $\rho_{1h} = (\pm 0.93770;\ 0)$, $\rho_{1e} = (\pm 3.68926;\ 0)$. In figures 5(a) and (b), where $\omega_0 = 0.5$ and $\omega_0 = 0.3$, respectively, the value Δ_+ exceeds $\Delta_{\max}$, and hence there are no stationary points on the y-axis. As can be seen from the figures, the sizes of all circulation cells along the y-axis increase with decreasing ω_0. A pair of degenerate stationary points and an external separatrix associated with them are shown in figure 5(c), where an example with $\Delta_+ = \Delta_{\max}$ is given. Figure 5(d) shows the separatrix for the reconnection case – (case (1.1) of figure 2); and figure 5(e) shows the separatrix for the case of motions of class S (the values of s_0 here are the same as in the lower line in figure 2); figure 5(f) shows the separatrix for the case $s_0 = 0$.

The latter example is of interest due to the fact that the circular trajectories, which are not separatrices in this case, feature a change in their cyclonic type. Starting from inverse roundabout with dominating intralayer interaction, they change to an ordinary roundabout, where the vortices in the lower layer rotate in the direction induced by the upper layer anticyclone, and finally back to an inverse roundabout (now, under the effect of the cyclonic component of the external field). Note that, in figure 4(d),

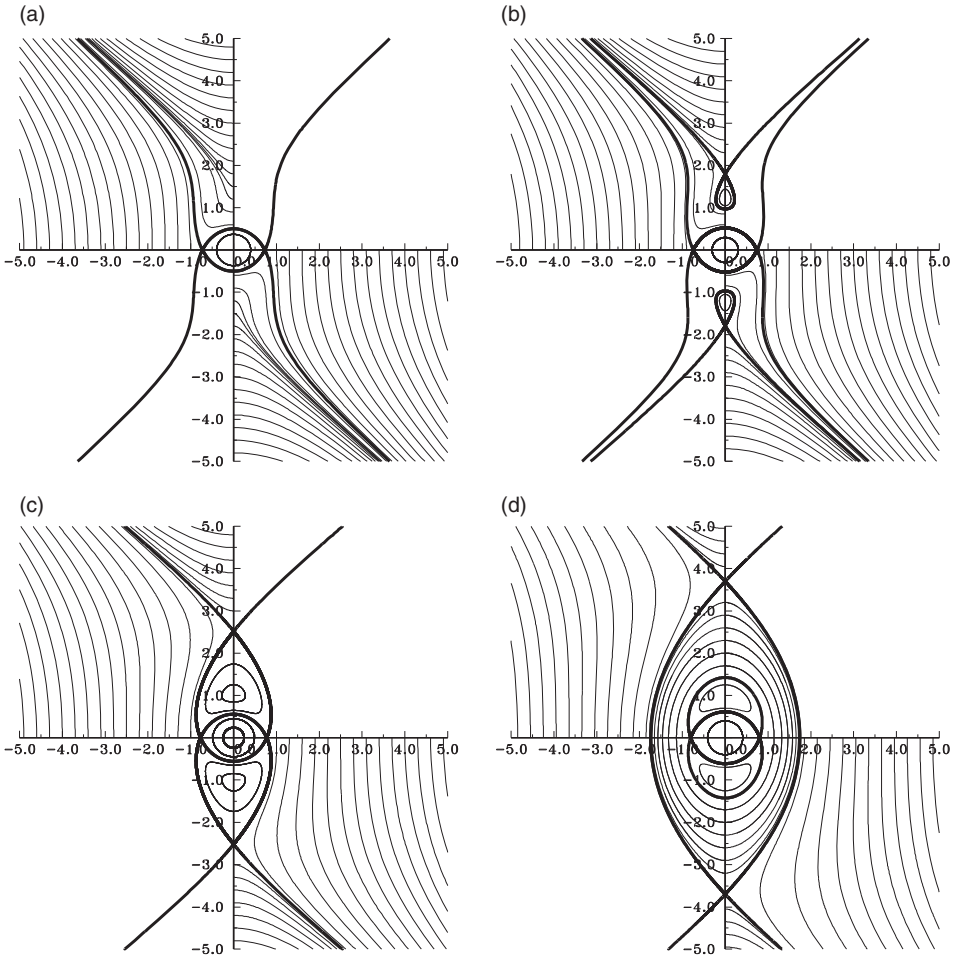

Figure 6. Bottom-layer vortex trajectories issued from initial positions on the x- and y-axes at $\omega_0 = 0$: (a) $s_0 = 0.30$, $\rho_{1h} = (\pm 0.72845; 0)$; (b) $s_0 = 0.25$, $\rho_{1h} = (\pm 0.74490; 0)$, $\rho_{2e} = (0; \pm 1.21069)$, $\rho_{2h} = (0; \pm 1.78998)$; (c) $s_0 = 0.17759$, $\rho_{1h} = (\pm 0.77168; 0)$, $\rho_{2e} = (0; \pm 1.03044)$, $\rho_{2h} = (0; \pm 2.51862)$; (d) $s_0 = 0.10$, $\rho_{1h} = (\pm 0.80539; 0)$, $\rho_{2e} = (0; \pm 0.93727)$, $\rho_{2h} = (0; \pm 3.69914)$ (triangular markers in figure 3). Thick trajectories coincide with separatrices.

where the radii of those two circles coincide as a result of reconnection, the ring domain for ordinary roundabout degenerates into a circle of stationary positions of lower layer vortices. This is confirmed by the medium curve of figure 1(c); this curve can be interpreted as the dependence $\omega_0(\rho_0)$ at $s_0 = 0$. According to this figure, at $-\infty < \omega_0 \leq 0$ there always exists one stationary state of the roundabout on a circle with radius ρ_0, while at $0 < \omega_0 < \Delta_{\max} = 0.27094$ there will be two stationary states on circles with radii $\rho_{01} \leq \rho_{02}$, where $\rho_{02} \to \infty$ at $\omega_0 \to 0$ and $\rho_{01} = \rho_{02} = \rho^* = 1.4407$ at $\omega_0 = \omega_0^* = 0.27094$. When $\omega_0 > \omega_0^*$, the angular velocity of the roundabout is positive everywhere.

The influence of parameter s_0 on lower layer vortex dynamics, for $\omega_0 = 0$, is shown in figure 6. In addition to separatrices, this figure also shows the trajectories of vortices from their initial positions on the x- or y-axes. When the external shear is strong enough, (see figure 6(a), where $\Delta_- < 0$, and $\Delta_+ > \Delta_{\max}$), there exists only one pair of

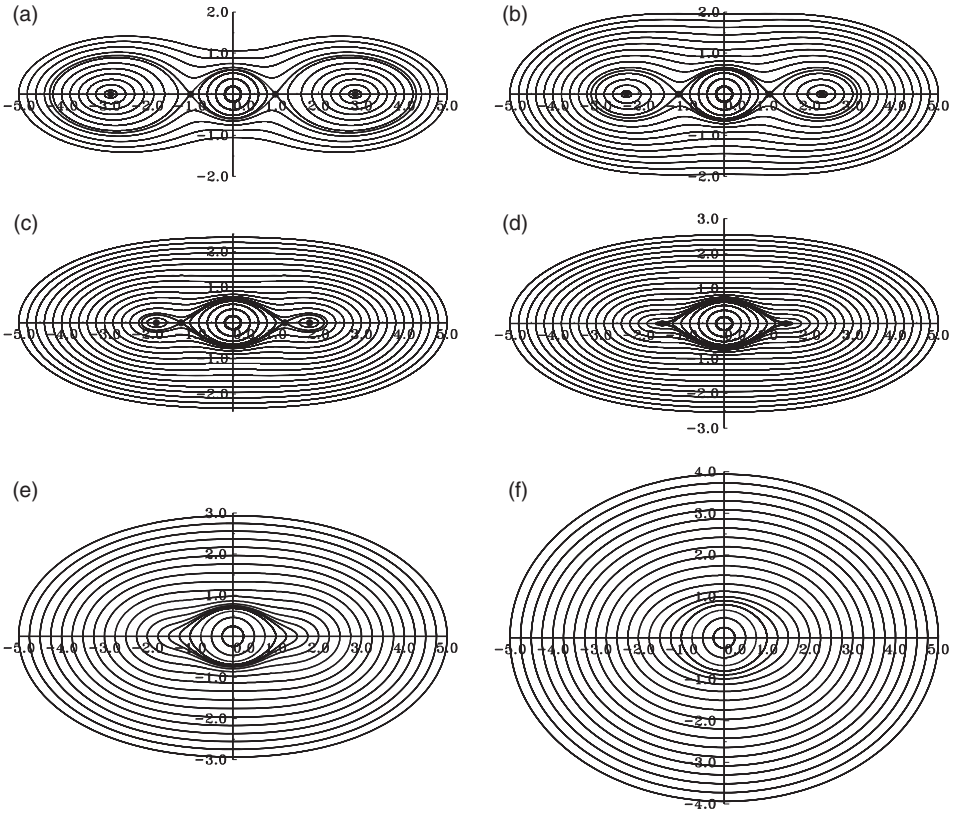

Figure 7. Bottom-layer vortex trajectories issued from initial positions on the x- and y-axes at $\omega_0 = 0.5$: (a) $s_0 = 0.35$, $\rho_{1h} = (\pm 0.99183; 0)$, $\rho_{1e} = (\pm 2.85344; 0)$; (b) $s_0 = 0.30$, $\rho_{1h} = (\pm 1.06911; 0)$, $\rho_{1e} = (\pm 2.28190; 0)$; (c) $s_0 = 0.25$, $\rho_{1h} = (\pm 1.21069; 0)$, $\rho_{1e} = (\pm 1.78998; 0)$; (d) $s_0 = 0.22906$, $\rho_{1h} = \rho_{1e} = (\pm 1.44087; 0)$; (e) $s_0 = 0.20$; (f) $s_0 = 0.10$ (square black markers in figure 3).

stationary hyperbolic points on the x-axis. In this case, closed trajectories are contained within a small central domain, while the vortices outside it are carried away by the external flow. In figure 6(b), where $\Delta_+ < \Delta_{\max}$, there are two pairs of singular points – elliptic and hyperbolic – on the y-axis. In this pure shear flow, a remarkable fact is the appearance of upper and lower closed domains which form via the capture of lower layer vortices by the upper anticyclone; in this case, the capture domains are isolated from the central domain by a narrow zone of infinite vortex motions. The tendency toward such a capture becomes stronger with a gradual decrease in s_0: figure 6(c) gives the case of reconnection; figure 6(d) is an analog of motions of class S with a closed internal separatrix and an external domain with respect to this separatrix, which contains finite anticyclonic motions along a common trajectory.

Figure 7 presents a series of results of numerical experiments to study the effect of s_0 at finite ω_0 ($\omega_0 = 0.5$). Here all trajectories of lower layer vortices are closed. When $\Delta_- < \Delta_{\max}$ (panels (a)–(c)), there are two pairs of singular points on the x-axis, and the set of trajectories takes the form of three cells of closed cyclonic circulations imbedded in a cyclonic external flow. When $\Delta_- = \Delta_{\max}$ (panel (d)), the singular points merge, thus yielding two fixed points. Note that in this case, $\rho_e = \rho_h = 1.44087$, which clearly

coincides with the value ρ^* in figure 4(d), since the corresponding points in figure 3 lie on the same line $\Delta_- = \Delta_{\max}$. A further decrease in s_0 (i.e. an increase in Δ_-) results in the formation of a system of centered, imbedded trajectories with cyclonic rotation of lower layer vortices. Considering the panels of this figure in reverse order shows that an increase in s_0 results in the first appearance of a curve with zero rotation frequency of lower layer vortices at $\Delta_- = \Delta_{\max}$; later this curve transforms into a heteroclinic separatrix, which can also be considered as two homoclinic separatrices with whiskers joining around the central domain, and running around the three-cell structure of closed circulations.

In the following section, we will analyze vortex rotation frequencies in the lower layer versus the distance between them and the central vortex of the lower layer. This study is directly related to the emergence of chaotic regimes for vortices when the external flow has an unsteady component.

4. Analysis of optimal frequencies of perturbations

Chaotic regimes in dynamic systems are determined by the geometric characteristics of the nonlinear resonance domains (Koshel and Prants 2006, 2008, Zaslavsky 2007, Perrot and Carton 2009). Their evaluation requires the knowledge of the rotation frequencies of vortices along the closed trajectories. This allows the determination of parameters of the unsteady external flow, which are optimal for the appearance of chaotic regimes (Izrailsky *et al.* 2006, 2008) or for the manifestation of some specific effects of chaotization (Koshel *et al.* 2008).

Figure 8 gives the dependence of rotation frequency ν for lower layer vortices on their initial position x_0 or y_0 on the x- or y-axis for some sets of trajectories of figure 2. Clearly, zero values $\nu(x_0)$ or $\nu(y_0)$ are attained on separatrices.

It is often convenient to shift to action-angle variables, so that each trajectory in the undisturbed system will be uniquely determined by the value of the action variable. Since such a change is difficult in our problem, we identify the trajectory by its initial position x_0 or y_0. These initial coordinates uniquely determine the trajectory, i.e. there exists a one-to-one correspondence between x_0 or y_0 and the action. Note that by the rotation frequency at x_0 we mean the value $\nu(x_0) = \mathrm{sgn}(\varpi)2\pi/T(x_0)$, where T is the period, and ϖ is the angular velocity, which, unlike $\nu(x_0)$, is not constant along the trajectory.

Following Zaslavsky (2007), we say that the nonlinear resonance established on a trajectory with rotation frequency $\nu(x_0) = (m/n)\nu^*$ has a rotation number m/n. The integer variable n equal to the number of islands (elliptic and hyperbolic points) will be referred to, as resonance multiplicity, and m, i.e. the number of periods during which the trajectory travels over all islands, will be called the resonance order. Here ν^* denotes the frequency of the unsteady perturbation, which will be chosen from the analysis of frequency relationships (as, e.g. in figures 8 and 9).

Let us assess the parameters at which the formation of chaotic regimes and chaotization domain is possible (Izrailsky *et al.* 2006, 2008, Koshel *et al.* 2008). Note that the modulus of the maximum rotation frequency in closed central, peripheral, and flow-through domains has the order of $\nu \sim 0.004$–0.020. Since the domains of nonlinear resonance 1 : 1 are commonly the largest in the system, the value of the

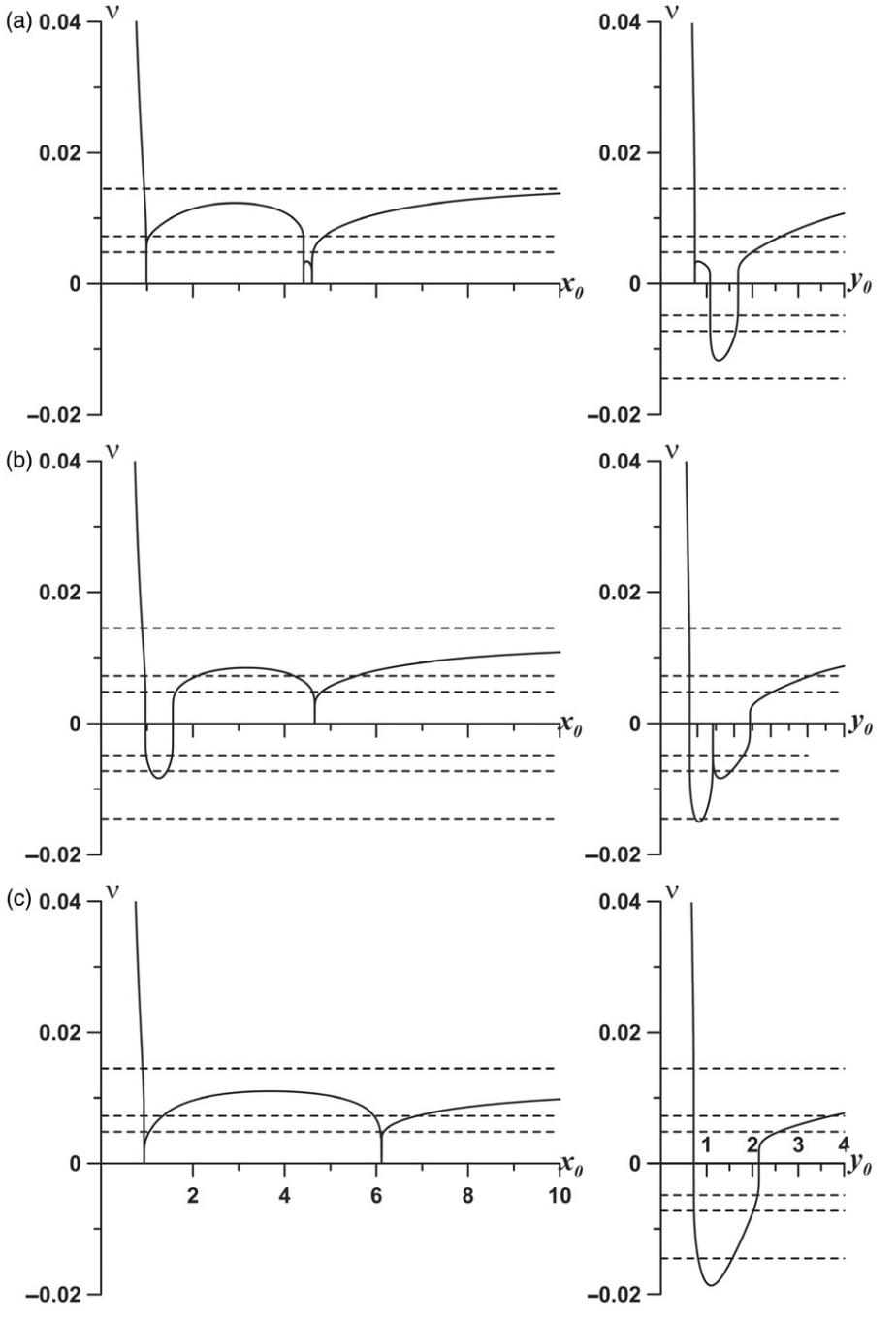

Figure 8. Dependence of lower layer vortex rotation frequencies on the initial position on the x- or y-axis. The estimates are given for characteristic cases of figure 2: (a) (1.2); (b) (2.1); (c) (1.1). The dashed lines show the levels $\nu = 0.0145$, $\nu/2$, $\nu/3$.

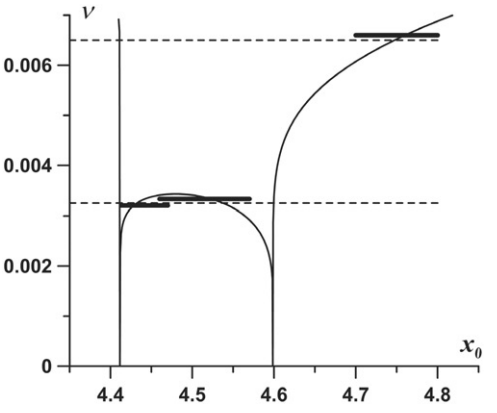

Figure 9. Enlarged fragment of case (1.2) of figure 8(a) (left). The dashed lines show levels $\nu^* = 0.065$ and $\nu^*/2$. Thick segments show the domains of x-coordinates of the trajectories involved in nonlinear 1 : 1 resonance (in the external domain) and two nonlinear 1 : 2 resonances (in the closed flow-through domain).

unsteady-perturbation frequency for the generation of sufficiently effective chaotization is generally taken to be somewhat smaller than the maximum rotation frequency.

In the examples considered here, the domain between the separatrices is narrow and the domains of closed circulations along the y-axis are also small, while the large resonance 1 : 1 produces considerable deformations in the trajectories in those domains. Therefore, we will choose the perturbation frequency in numerical experiments such that its half is smaller than the maximal rotation frequency. Such a choice will allow us to identify more vividly the effects of chaotization, which will be determined by the positions of resonances of the 1 : 2 type. These latter resonances, the perturbation amplitude being the same, have much smaller width in terms of frequency than the 1 : 1 resonance.

It is worth mentioning that, in the domains containing an elliptic point, a single trajectory corresponds to each rotation frequency and that the maximum frequency is attained at the elliptic point. In closed domains lying between different separatrices, the maximum frequency corresponds to the closed trajectory, and two trajectories correspond to frequencies smaller than the maximum.

First, we will consider the perturbation which causes chaotization in the neighborhood of separatrices but which does not destroy the regular barrier between separatrices in the closed domain. This will allow us to illustrate the emergence of a transport barrier between the internal and external domains in the phase portrait. To implement such a scenario, let us assume that $\nu^* = 0.01450$, for which $\nu^*/2$ will be smaller than the maximal frequency in all closed domains, but larger than the maximal frequency in the domain between separatrices (in the (1.2) case, even $\nu^*/3$ will be larger than this latter value). The above reasoning is illustrated by figure 8, where the levels of ν^*, $\nu^*/2$ and $\nu^*/3$ are represented by dashed lines. The intersections of those lines with the rotation frequency curve yields the x- or y-coordinate of the intersection points of the resonance trajectory with the appropriate coordinate axis, i.e. the required values x_0 or y_0. With such a choice of perturbation parameters, the trajectories corresponding to the 1 : 1 resonance exist only in closed domains; they are localized near elliptic points and located far enough from trajectories of 1 : 2 resonances. Therefore, we can expect only overlapping of 1 : 2 and 1 : 3 resonance domains or (if the perturbation amplitude is

sufficiently small) 1 : 3 and 1 : 4 resonance domains (Izrailsky *et al*. 2006, 2008). In this case, there exists a probability that a narrow stochastic layer will appear in the neighborhood of separatrices; the closed domains and, more significantly, the domain between separatrices, will remain mostly regular (Izrailsky *et al*. 2008). In such a situation, a regular barrier should persist in this domain. However, in the case of separatrix reconnection, the stochastic layers will merge, forming a chaotic transport passage from the internal to the external domains.

The regular barrier described above can be destroyed not only via a reconnection of separatrices, but also via an increase in the perturbation amplitude or, more interestingly, with a successful choice of perturbation frequency corresponding to reconnection of nonlinear resonances of the same order in the neighborhood of the trajectory with maximal rotation frequency, the perturbation amplitude being small enough.

This situation is illustrated in figure 9, where thick segments show the initial positions of trajectories involved in 1:2 resonances in the closed domain between the separatrices, and 1 : 1 resonance in the external domain at the perturbation frequency $\nu^* \sim 0.0065$. We can see that at such perturbation frequency, two resonances of 1:2 type are close to the trajectory with maximal rotation frequency, and reconnection of their separatrices takes place at some perturbation amplitude (Koshel *et al*. 2008). As a result, a chaotic transport passage should appear between the separatrices. The domains of 1 : 2 resonances are close to both separatrices, but the trajectory with maximal rotation frequency is located close to the internal one; therefore, the corresponding resonances 1 : 2 and 1 : 3 should completely overlap. On the side of the external separatrix, the distance between the same resonances is larger, hence the overlap will be only partial. In this internal domain, the 1 : 2 resonance will be completely destroyed because of overlap with the internal 1 : 3 resonance, while the external 1 : 2 resonance will be only partially destroyed, though sufficiently for a new transport passage to form.

5. Transition to chaos

The analysis of rotation frequency along trajectories allowed the prediction of some effects of chaotization for unsteady external flow. In this section, we will check the analysis above by direct calculations. To identify the domains and the major effects of chaotization, results are presented in Poincaré sections. In view of symmetry, only one vortex position in the lower layer will be shown once every perturbation period. Only when necessary, the analogous information for the second vortex will be presented.

Figure 10 shows the case when the barrier is located in the domain between separatrices. The calculations shown here refer to parameters of cases (1.2), (2.1) of figure 2, i.e. before and after reconnection of separatrices, as well as to parameters of case (1.1), i.e. at the reconnection. As shown above, the perturbation frequency ($\nu^* = 0.0145$) was chosen from the condition that the barrier between separatrices should not be destroyed.

Suppose that

$$s(t) = s_0(1 + \varepsilon \sin \nu t), \quad \omega(t) = \omega_0(1 + \varepsilon \sin \nu t), \tag{21}$$

where $\varepsilon = 0.01$.

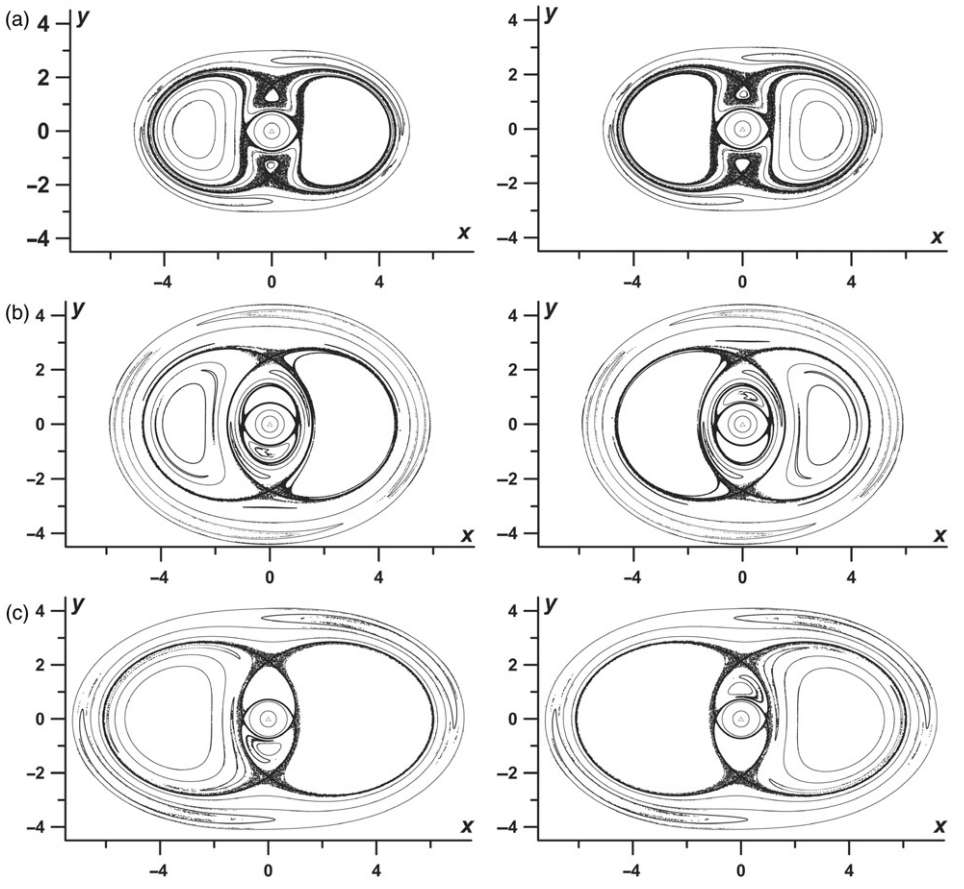

Figure 10. Poincaré section for the left (in terms of the initial position) and right vortices of the lower layer for the same cases as those shown in figure 8. In all cases, the perturbation frequency $\nu^* = 0.0145$, and the amplitude $\varepsilon = 0.01$. Undisturbed separatrices are shown from figure 8: (a) (1.2); (b) (2.1); (c) (1.1). The symbols for chaotic domains and nonlinear resonances are somewhat larger than those for quasi-regular trajectories.

In all cases we observe irregular behavior of vortices in the neighborhood of separatrices, with periodic flip-overs† between the domain between separatrices, the closed domains of the internal separatrix and the domain out of the external separatrix. At the same time, the regular barrier in the domain between separatrices hampers flip-overs from the neighborhoods of the internal separatrix into the external domain.

The flip-over processes are vividly illustrated in figure 11, where dependence of $x(i)$ or $y(i)$ on i are shown; here i is the number of the perturbation period for the appropriate parameter sets. Characteristic types of vortex motions can be easily identified. For irregular variations of the vortex coordinate in the stochastic layer, regimes can be seen

†The notion of "flip-over" between different motion regimes was first introduced by Gluhovsky and Klyatskin (1977); see also Klyatskin 2008.

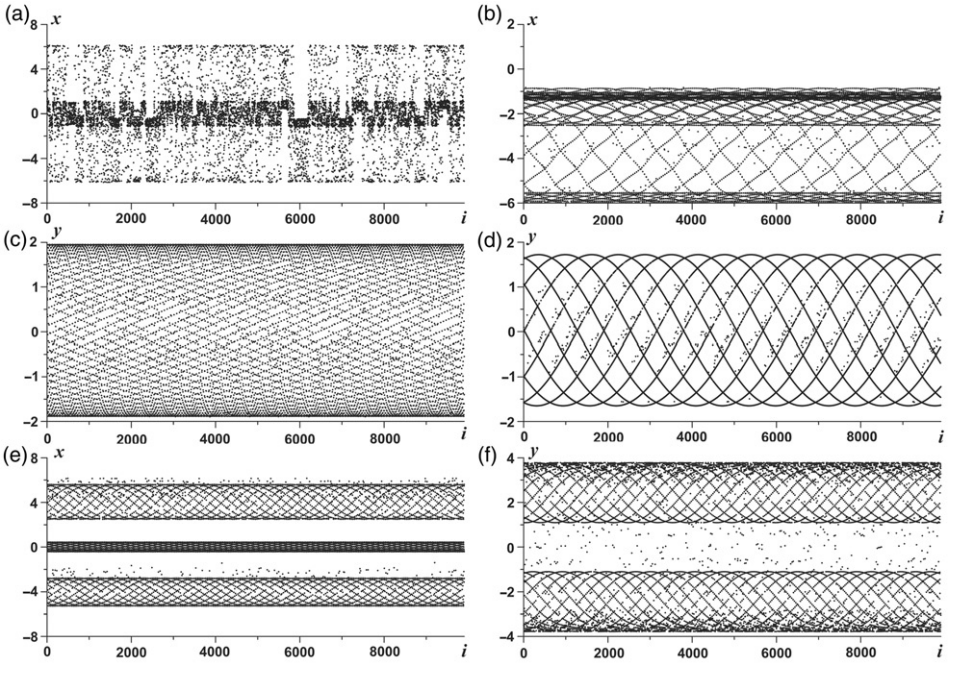

Figure 11. Dependence of $x(i)$ or $y(i)$ on i for lower layer vortex in the (1,1) case of figure 10 for different initial positions. The panels correspond to the following regimes of lower layer vortex motions: (a) vortices in the chaotic layer in the neighborhood of the separatrix; (b) vortices in the 1 : 2 nonlinear-resonance domain in lateral vortex domains; (c) and (d) quasi-regular behavior in lateral vortex domains; (e) 1 : 3 resonance on the external boundary of the stochastic layer; (f) 1 : 2 resonance in the external domain.

where the vortex

(a) lies in the right (left) closed domain – as determined by the position in the positive or negative domain of $x(i)$ values,
(b) lies in the top (bottom) closed domain – by small amplitudes of variations in the y-coordinate,
(c) moves within the internal or external domain – by sign-variable coordinate values with characteristic minimal (in the former case) or maximal (in the latter case) amplitudes.

If the trajectories are captured by the nonlinear resonance areas, two or three domains of coordinate variations can be clearly seen and the overall behavior is practically regular. In regular domains, the vortex passes through the entire interval of coordinate variations, and the number of regular segments of curves corresponds to the ratio of rotation frequency of the trajectory to the perturbation frequency.

An interesting effect that can be identified in the analysis of one coordinate is that even nearly regular trajectories are destroyed, as slightly as may be, by high-multiplicity resonances, which are too small to be resolved in such calculations. This latter effect is manifested by the presence of a small number of irregular positions in the corresponding figures. The intervals of irregular behavior are obviously very rare in such cases.

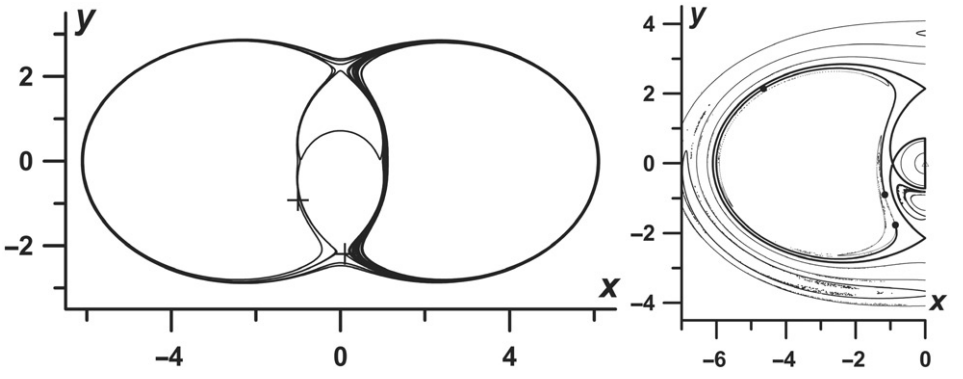

Figure 12. Segments of trajectories from the stochastic layer (left) and from the 1 : 2 resonance domain (right) – for case (1.1) of figure 10. Symbols (+) mark the beginning and the end of the stochastic trajectory and the position of the resonance trajectory (black circles) after each perturbation period $T = 2\pi/|\nu^*|$. Since the resonance trajectory does not leave the left vortex domain, only half of the figure is shown; the trajectory of the second vortex of the lower layer is located symmetrically in the right vortex domain.

Quasi-regular segments of trajectories in the domains between flip-overs are shown in figure 12. Here a vortex makes several quasi-regular rotations in the right closed domain, then it changes type of motion and makes two rotations in the external domain; then it makes a rotation in the top closed domain and passes into the left closed domain. The same figure shows a segment of the trajectory belonging to the zone of 1 : 2 resonance. The second trajectory shows that this vortex, after the perturbation period, reaches a trajectory belonging to one of the resonance stability islands in the Poincaré section, and, after an odd number of periods, the trajectory reaches the second stability island. In other words, during the relative motion along an undisturbed trajectory with frequency $\nu^*/2$, the vortex moves along one of the two closed (perhaps, partially destroyed) trajectories of Poincaré section belonging to that resonance. The situation with resonances of other orders is similar, except that the vortex visits each closed trajectory only once every n period, where n is the order of the resonance. In the case of fractional resonances, i.e. when the rotation frequency ratio of the resonance trajectory to the perturbation frequency of the form $\nu(x_0)/\nu^* = m/n$, where m and n are integers, the situation is more complex (see, e.g. Koshel *et al.* 2008).

Thus, the stochastic trajectory originates in the neighborhood of the lower hyperbolic point (the origin is marked by a cross). Then it is captured by the right vortex domain, where it makes several rotations, after which a flip-over into the external domain takes place; after two rotations, the trajectory penetrates, along the internal part of the separatrix, into the upper vortex domain and, after one rotation in this domain, it passes into the left vortex domain (the end of the trajectory is also marked by a cross). The regular trajectory always stays in the left vortex domain, and visits one of the 1 : 2 resonance islands once every period. The origin of this trajectory is marked by a black circle and belongs to the trajectory of Poincaré section in the lower stability island; its position after one period is also marked by a black circle in the upper island; and after the following period, the third black circle again lies within the lower island. We showed only half of the phase portrait for this trajectory, since the vortex did not leave the left vortex domain. Note that the motion of the second vortex in the lower layer is symmetrical about the origin of the plane.

In the case of reconnection of separatrices (case (1.1) in figures 8 and 10) a vortex having entered the near-separatrix stochastic layer is involved in motions of all possible types (an example is given in figure 12); in particular, it can move from the neighborhood of the internal domain into the external domain and back into internal one. Figure 12 gives two examples of trajectories, one of which is chaotic and the other is regular. Dependence $x(i)$ for this case, given in figure 11, shows that flip-overs between motion regimes are frequent; therefore vortices do not penetrate deeply into closed domains, though the actual thickness of the stochastic layer is somewhat larger than that obtained for the present initial position of the vortex. We can see that, in the case of reconnection of separatrices, the lower layer vortex can either move in the central domain (in a very thin near-separatrix layer) or penetrate into the external domain, i.e. the pattern of vortex behavior becomes much more complex.

The above analysis shows that, as was the case with passive tracers (Izrailsky *et al.* 2006, 2008, Koshel *et al.* 2008), the major effects of chaotization and the parameters for its appearance can be identified via the undisturbed rotation frequencies of lower layer vortices.

Now, we consider another effect, which has been analyzed in detail in Koshel *et al.* (2008), namely the reconnection of nonlinear-resonance separatrices in a closed domain between separatrices. In previous calculations, we intentionally chose the perturbation frequency such that $\nu/3$ is somewhat larger than the maximum rotation frequency in the domain considered (see figure 8). Now we render the perturbation frequency somewhat smaller than this maximum. For $\nu = 0.0065$, 1:2 resonances are possible in the closed domain between separatrices (see figure 9), close to the trajectory with maximal frequency (one trajectory lies within it and another one outside it). Accordingly, when those resonances are sufficiently wide, their separatrices can also be subject to reconnection, resulting in chaotization of the central part of the domain. Then, if those resonances overlap with 1 : 3 resonances located near separatrices, a chaotic flip-over becomes possible through that layer, from inside the internal separatrix to the external domain. Another feature is that the distance between 1 : 2 and 1 : 3 resonance domains is smaller in the internal than in the external part of the closed flow-through domain, i.e. the degree of their overlap will be different.

The above effects are illustrated in figure 13. In agreement with the rotation frequency analysis, chaotic behavior occurs in the closed domain between separatrices, except for two islands of regular behavior, near the external separatrix and corresponding to a 1 : 2 resonance. Thus, the destruction of the regular barrier between

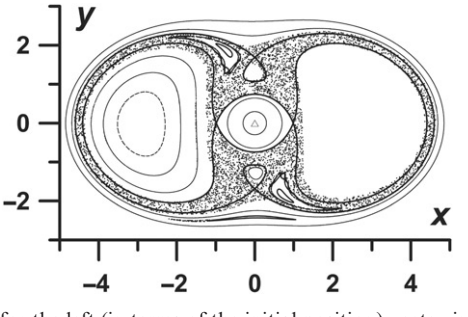

Figure 13. Poincaré section for the left (in terms of the initial position) vortex in the lower layer; parameters of figure 9 ($\nu^* = 0.0065$, $\varepsilon = 0.01$). Undisturbed separatrices from figure 8 are given.

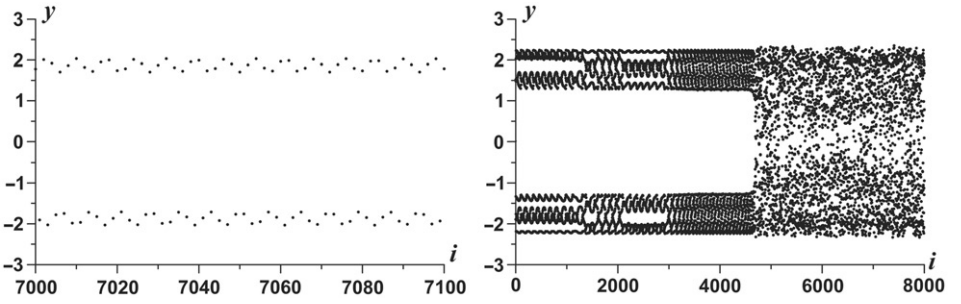

Figure 14. Dependence of $y(i)$ on i for a regular trajectory from the island of regular behavior corresponding to 1 : 2 resonance in the flow-through domain (left) and for a vortex with initial position in the stochastic layer of the flow-through domain (right). Parameters are of figure 13.

the external and internal domains can be implemented by a choice of parameters facilitating either reconnection of major separatrices, or reconnection of separatrices of nonlinear resonances near the barrier.

The same calculation allows us to see an important effect of ''adhesion''†, which is closely related to ''Levi flights'' (Solomon *et al*. 1994). Figure 14 shows the dependence $y(i)$ for two trajectories, one in the domain of the stability island, corresponding to the incompletely destroyed 1 : 2 resonance, and the other in the chaotic domain.

In the quasi-regular dependence (the left part of the figure), each stability island of this resonance is visited; therefore, we see two trajectories: one refers to even periods and corresponds to one island, and the other one refers to odd periods and corresponds to the second island. The quasi-sinusoidal form of each dependence corresponds to the motion along the Poincaré section trajectory within the island. A small segment of this trajectory is shown here, but it preserves its form over 12,000 perturbation periods (i.e. nearly indefinitely).

The right-hand part of figure 14 corresponds to an initial position in a thin stochastic layer, which surrounds secondary resonances at the periphery of stability islands (Zaslavsky 2007). In the initial, rather long stage (of the order of 5000 perturbation periods), the dependence looks quasi-regular. It consists of several regular segments, but at several random instants, it performs flip-overs between different regimes in the neighborhood of 1 : 2 resonances; finally, the motion becomes strongly chaotic.

One more example is shown, where the stochastic layer can be appreciably extended for a proper choice of the perturbation frequency, keeping its same amplitude. For case (1.1) of figure 10, all zones of resonance (1 : 1 in the bottom and top domains, 1 : 2 in the left, right, and external domains) are localized not very far from the stochastic layer. Therefore, even an insignificant decrease in perturbation frequency should make them closer to the stochastic layer (see figure 8).

In view of the estimate of Zaslavsky (2007):

$$\frac{\nu^*}{n} - \frac{\nu^*}{n+1} = \frac{\nu^*}{n(n+1)} = \nu(x_0|_{1:n}) - \nu(x_0|_{1:(n+1)}) \sim \frac{\mathrm{d}\nu(x_0)}{\mathrm{d}x_0}\left(x_0|_{1:n} - x_0|_{1:(n+1)}\right) \qquad (22)$$

†As far as we know, Zaslavsky (2007) was the first to discuss the effect of ''adhesion'' or ''stickiness'' of islands.

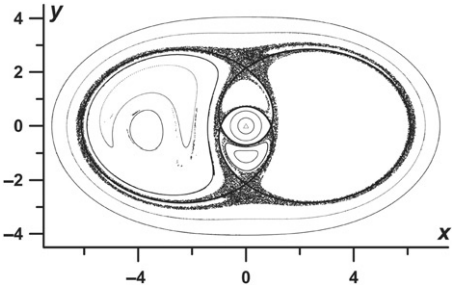

Figure 15. Poincaré sections for the left (in terms of the original position) vortex of the lower layer, with parameters of case (1.1) of figure 8 ($\nu^* = 0.01$, $\varepsilon = 0.01$). Undisturbed separatrices from figure 8 are given.

the distance between neighboring resonances in terms of coordinate x

$$x_0|_{1:n} - x_0|_{1:(n+1)} \sim \frac{\nu^*}{n(n+1)} \Big/ \frac{\mathrm{d}\nu(x_0)}{\mathrm{d}x_0} \tag{23}$$

will significantly decrease, since the derivative of the rotation frequency with respect to the coordinate increases when approaching the separatrix, while the frequency itself varies insignificantly. As a result, the above resonances will overlap with stochastic-layer resonances and their width will increase by the width of these resonance areas.

Assuming a perturbation frequency $\nu^* = 0.01$, the results shown in figure 15 indicate that the extension of the stochastic layer really takes place. The calculations above show that our dynamical system allows the application of practically all mechanisms of chaotization known from the analysis of passive markers of lower layer vortices.

One more effect can be examined with the cases given in figures 4(d) and 5(f). An interesting feature of these cases is that they have no hyperbolic singular points, but a curve with a peak in rotation frequency (this mechanism was considered above for another case); their feature of particular importance is the presence of a curve (or two curves) with zero rotation frequency. The corresponding frequency relationship is given in figures 16(a) and (c).

In this case, $s_0 = 0$; therefore, we consider a perturbation in the form

$$s(t) = \varepsilon \sin \nu t, \quad \omega(t) = \omega_0(1 + \varepsilon \sin \nu t). \tag{24}$$

The analysis of figure 16(a) shows that, first, trajectories with zero rotation frequency will clearly serve as quasi-separatrices, since their neighborhood, as well as the neighborhoods of ordinary separatrices, contains many nonlinear resonances with rotation numbers $1:n$, whose overlapping should result in the appearance of a stochastic layer. Second, by appropriately choosing the frequency (see figure 16(a)), we can place nonlinear resonances (in this case, $1:2$) near the external trajectory with zero rotation frequency (inside and outside); if these resonances overlap with the stochastic layer, its width will increase considerably. The Poincaré section given in figure 16(b) completely illustrates this mechanism. In this figure, a narrow stochastic layer lies in the neighborhood of the internal separatrix, and a stochastic sea is associated with the overlapping of the internal and external $1:2$ resonances in the neighborhood of the external quasi-separatrix.

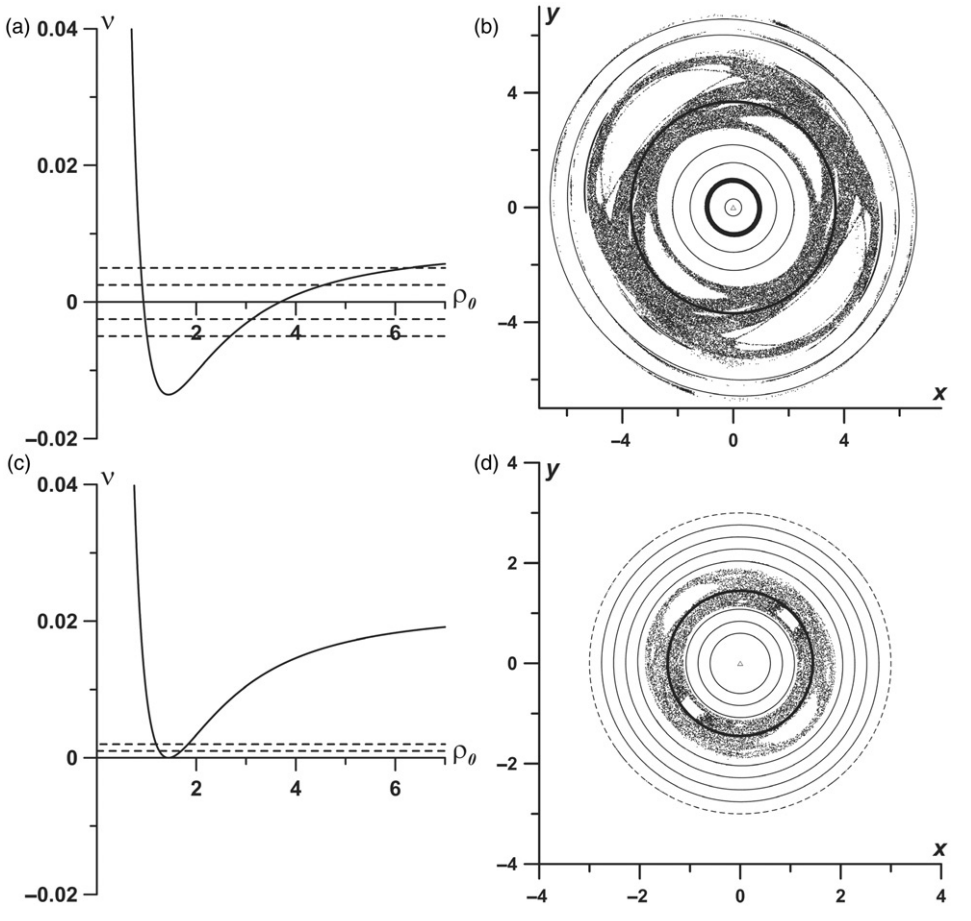

Figure 16. Dependence of rotation frequency (left) and Poincaré section (right) for parameters of figure 5(f) ($\omega_0 = 0.10045$, $s_0 = 0$)–(a) and (b) and figure 4(d) ($\omega_0 = 0.270940$, $s_0 = 0$)–(c) and (d). The levels shown in frequency dependences are as follows: (a) $\nu^* = \pm 0.005$ and $\nu^*/2$; (b) $\nu^* = 0.002$ and $\nu^*/2$. Perturbation amplitudes: (b) $\varepsilon = 0.005$; (d) $\varepsilon = 0.003$.

Two more important points are worth mentioning:

- The motions of vortices between and outside the separatrices have different directions, i.e. vortices can change the direction of their motion in chaotic domains and stop for some time.
- As it is known from the theory of dynamic chaos, the thickness of the stochastic layer in the neighborhood of a hyperbolic point is larger than in other parts of the separatrix. However, in our case, it is uniform all along the internal separatrix.

In particular, if a hyperbolic point exists at zero perturbation, the thickness of the stochastic layer is of the order of $\sqrt{\varepsilon}$ in its neighborhood and the order of ε all along the rest of the separatrix (Lazutkin 1989). Note that the cases where a hyperbolic point exists in a stationary system and where it appears only at a nonzero perturbation are essentially different. In the latter case, the stochastic layer is commonly

exponentially thin. There is no conclusive answer still as to what case this example belongs. The question that naturally arises requires special consideration: *what is the order of the stochastic layer thickness in the neighborhood of separatrix that does not have a hyperbolic point?*

Calculations for the case of a single zero-frequency curve are given in figures 16(c) and (d). In this case, the vortices move in the same direction both inside and outside this trajectory: we have only a minimum (zero) on the frequency relationship. Resonances of the same order can exist on both sides of this curve, resulting in the overlapping of domains of sufficiently large resonances (here, these are 1 : 2) and the formation of sufficiently wide chaotization domain. However, the question is still open as to whether a stochastic layer can form as the result of reconnection of separatrices for resonances of the same order *in the neighborhood of the minimal-frequency curve at arbitrary frequency and amplitude*.

Finally, let us consider a case, similar to cases in figure 6, when there is no rotational component of the external field. An important feature of this case is the presence of infinite trajectories of vortices. In the stationary case, for vortices initially located on the x- and y-axes, several types of motions can occur for lower layer vortices: they can rotate around the upper vortex in the central domain; can remain in the capture domains, while rotating around elliptic points of the upper and lower closed domains or in the flow-through domain between separatrices; or they can move to infinity along the separatrices given in figure 6. However, if the initial positions of the vortices are sufficiently far from the center in the first and third quadrants of the (x, y) domains, then, after approaching the neighborhood of the domain bounded by the separatrices whiskers, they move away to infinity.

In the unsteady case, if we take the initial trajectories near separatrices but far enough from the central domain and if we choose a perturbation that results in effective chaotization, the vortices can be captured for some time by closed domains.

Figure 17 illustrates the situation when lower layer vortices are captured by closed domains, stay within them for some time, and then run away to infinity. In figure 17(a) two lower layer vortices with the initial positions near the top right (black square) and bottom left (black circle) separatrix whiskers are captured by the top/bottom homoclinic loop, respectively; they stay within it for about 180 perturbation periods,

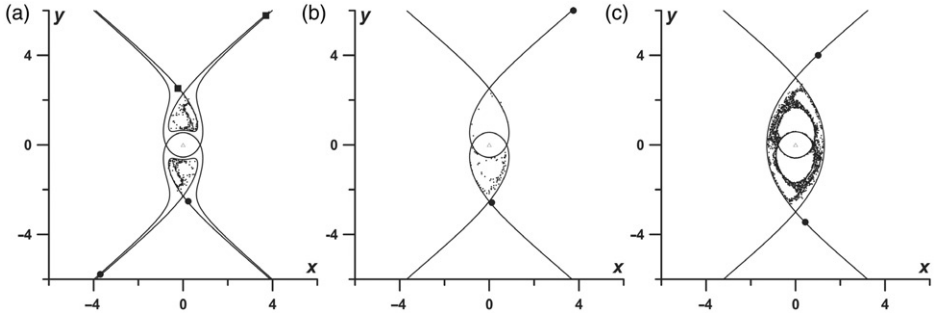

Figure 17. Poincaré sections for $\omega_0 = 0$ and the following values of parameters (a) $s_0 = 0.2$, $\nu^* = 0.03$, $\varepsilon = 0.05$ (the positions of both vortices in the lower layer are given, the black circle shows the initial and final positions of the left vortex, the square does the same for the right vortex); (b) $s_0 = 0.177590$, $\nu^* = 0.027560$, $\varepsilon = 0.05$ (a perturbed case of figure 6c); (c) $s_0 = 0.140$, $\nu^* = 0.030$, $\varepsilon = 0.033$.

and then they run away along the appropriate separatrices. The final positions of the vortices are marked by the same symbols. Intermediate positions of the vortices at each period are shown by point markers.

In panels (b) and (c), we give only the positions of one lower layer vortex, the position of the second one being centrally symmetric. Figure 17(b) shows a case with reconnection of separatrices. It differs from the previous case in that the vortex initially located in the upper part of the plane will be captured, as a rule, by a bottom lunate domain, and will stay in it for about 80 perturbation periods. Then it will be transferred into the top lunate domain, where it will make one and a half rotations, and only after that, run to infinity.

The situation in figure 17(c) differs in the presence (in the stationary case) of a zone of flow-through motions of vortices between separatrices; this zone commonly serves as a barrier for chaotic trajectories. However, this barrier can be easily destroyed by choosing parameters corresponding to reconnection of separatrices of nonlinear resonances in the neighborhood of the trajectory with maximal rotation frequency. Here the value $\nu^* = 0.016$ corresponds to the maximal rotation frequency in the domain between separatrices. It would be reasonable to use a perturbation with a frequency of the order of $\nu^* = 0.015$; however, the choice of $\nu^* = 0.03$ is optimal for the creation of the following conditions: (a) reconnection of the internal and external 1 : 2 resonance in the flow-through domain, (b) insignificant overlapping of the external resonance with the stochastic layer of the external separatrix, (c) formation of a dynamic trap. As can be seen from the figure, the vortex is first captured by the layer of the external separatrix, then it penetrates through the chaotic passage into the stochastic layer of the internal separatrix. It wanders during 1665 periods in the chaotic domain with regular flip-overs between the central zone and both lunate domains, sometimes visiting neighborhoods of resonances of flow-through domain. Finally, it leaves the trap and runs to infinity.

The influence of external flow parameter variation on the vortex system can be seen most conveniently in the vicinity of a reconnection. First, we examine a continuous (linear) transition between motions of types S and D: from case 2.1 to case 1.2 (along an auxiliary diagonal of figure 2), i.e. when

$$s(t) = \begin{cases} s_0(2.1) + \big(s_0(1.2) - s_0(2.1)\big)t/T & \text{for } t \le T, \\ s_0(1.2) & \text{for } t \ge T, \end{cases} \tag{25}$$

and

$$\omega(t) = \begin{cases} \omega_0(2.1) + \big(\omega_0(1.2) - \omega_0(2.1)\big)t/T & \text{for } t \le T, \\ \omega_0(1.2) & \text{for } t \ge T. \end{cases} \tag{26}$$

Here T is the time interval during which external parameters change from $s_0(2.1)$ and $\omega_0(2.1)$ to $s_0(1.2)$ and $\omega_0(1.2)$; the mentioned parameters values are taken from figure 2. Figure 18, where crosses mark the initial vortex positions, illustrates the lower layer vortex trajectories for such changes of the external flow. Vortices, being initially uniformly distributed inside the external separatrix, move to rather unexpected areas after they have passed the reconnection position: (1) three of them stay in their areas; (2) one vortex from the central domain and one from the external domain are found in the channel between separatrices; (3) other vortices run into the external area.

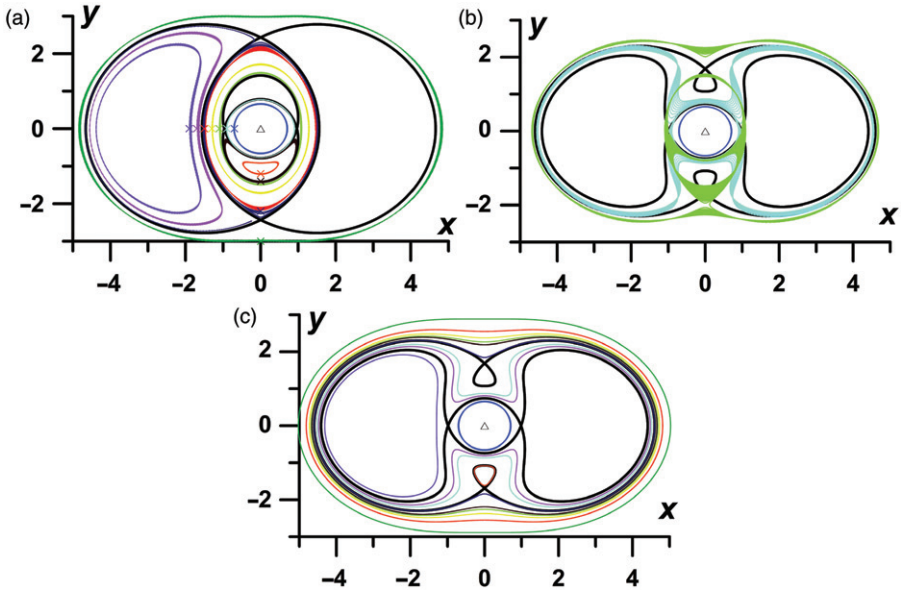

Figure 18. Vortex trajectories for the change of external flow parameters (25)–(26) at $T = 2\pi 10^4$. Each trajectory has its color, the same for all panels. (a) Initial parts of 10 trajectories during the time period from $t = 0.0$ up to $t = 0.1T$ (the behavior is close to case (2.1)), (b) only three trajectories over the time interval from $t = 0.0$ up to $t = 1.4T$, and (c) final calculated sections of all 10 trajectories over the time interval from $t = T$ up to $t = 1.4T$.

In this case, the system is integrable, and evidently time reversal would bring all vortices back to their initial positions.

A more complex case occurs when chaotization of vortex trajectories exists in the system. Consider an analogous transition from S to D and conversely, but with a periodic disturbance:

$$s(t) = \begin{cases} \big(s_0(2.1) + \big(s_0(1.2) - s_0(2.1)\big)t/T\big)\big(1 + \varepsilon \sin \nu t\big) & \text{for } t \le T, \\ \big(s_0(1.2) + \big(s_0(2.1) - s_0(1.2)\big)(t - T)/T\big)\big(1 + \varepsilon \sin \nu t\big) & \text{for } T \le t \le 2T, \\ s_0(2.1)\big(1 + \varepsilon \sin \nu t\big) & \text{for } t \ge 2T, \end{cases} \quad (27)$$

and

$$\omega(t) = \begin{cases} \big(\omega_0(2.1) + \big(\omega_0(1.2) - \omega_0(2.1)\big)t/T\big)(1 + \varepsilon \sin \nu t) & \text{for } t \le T, \\ \big(\omega_0(1.2) + \big(\omega_0(2.1) - \omega_0(1.2)\big)(t - T)/T\big)(1 + \varepsilon \sin \nu t) & \text{for } T \le t \le 2T, \\ \omega_0(2.1)\big(1 + \varepsilon \sin \nu t\big) & \text{for } t \ge 2T. \end{cases} \quad (28)$$

In this case, the initial positions are taken close to one another (the solid dot in figure 19 covers all vortex initial positions for corresponding calculations).

The points, whose initial positions lay in a very small area inside the stochastic layer near the internal separatrix (figure 19(a)) have run into unpredictable places of the phase space after the reconnection, during the first transition. During the second transition, the situation after the reconnection is even more interesting: (1) only one of ten vortices has come back into the initial stochastic layer, (2) one vortex is found in the stochastic layer near the external separatrix, (3) other vortices (in all areas, except the central one) have run onto periodic regular trajectories. Note that many trajectories

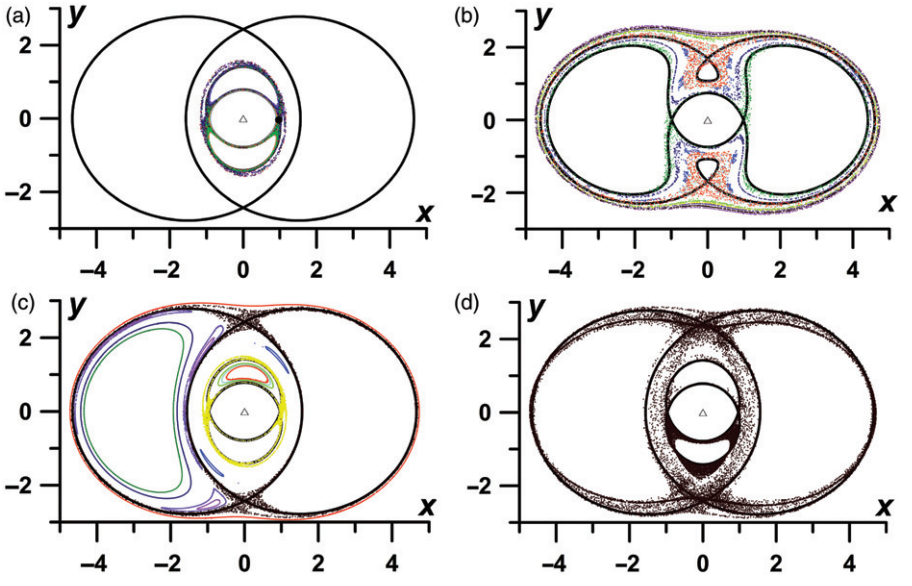

Figure 19. Vortex trajectories (in the sense of Poincaré sections) during the external-flow parameter change (25)–(26) at $T = 2\pi 10^4/\nu$, $\nu = 0.0145$ and $\varepsilon = 0.01$). Each trajectory has its color, the same for all panels. (a) The initial parts of trajectories in the interval from $t = 0.0$ up to $t = 0.1T$ (the behavior is close to case (2.1)), (b) trajectories in the time interval from $t = T$ up to $t = 1.1T$, (c) final trajectories parts in the time interval from $t = 2T$ up to $t = 2.4T$, and (d) example of a Poincaré section for one vortex during the whole time interval from $t = 0.0$ up to $t = 2.4T$.

have reached stability islands, corresponding to nonlinear resonances. This can be explained by the significant stability of resonance during the external flow changes; if the trajectory has penetrated into the evolving resonance area, it moves along with it.

6. Conclusions

This work presents a rather comprehensive study of steady tripolar point vortices in a regular external flow, in a two-layer rotating fluid. The role of external rotation and strain fields in the existence and evolution of stationary regimes was studied. In particular, the capture of peripheral vortices by the tripole core in a pure shear flow was demonstrated.

It was shown that with unsteady external flow (including small periodic perturbation), vortex motion acquires chaotic properties. Perturbation frequencies which are optimal for the formation of chaos were analyzed. The analysis results were confirmed by numerically constructing Poincaré sections. Examples were given to show the appearance of nonlinear resonances, the effects of flip-over between different regimes of vortex behavior, the phenomenon of vortex capture by chaotic domains, and the phenomenon of overcoming kinematic barriers.

Since Poincaré sections do not suffice to confirm the chaotization of trajectories, we demonstrated overlapping of resonances. The joint use of these two methods yields reliable results.

It is worth nothing that almost all significant features of dynamic chaos manifestations were revealed in the relatively simple problem of three vortex interaction in an external flow. Moreover, there is reason to believe that we found a new effect of the formation of a quasi-stochastic layer in the neighborhood of circular separatrices corresponding to zero rotation frequency. This layer may be due to reconnection of resonances of the same order.

The vortex systems under discussion in our work may have analogs in nature, as observed by satellite sensors. In the atmosphere, vortex compounds like omega blocks are imbedded in time-varying flows (Davis *et al*. 1993). In the oceans, the Mediterranean Water eddies southwest of the Iberian Peninsula (Carton 2001), the Southern Bay slope water oceanic eddies (Pingree and Le Cann 1992) or the Gulf Stream warm-core rings (Kennelly *et al*. 1985) can form baroclinic multipoles which are also subject to shear and strain induced by neighboring currents and eddies. Although hetons have been observed in the Antarctic Circumpolar Current (Savchenko *et al*. 1978), a generalization of this study to a baroclinic external flow should be carried out. But the stability of meddies or of Gulf Stream rings is due to their nonlinearity and to their finite size. The effect of this finite size on baroclinic multipole evolution in an external flow will be presented in a forthcoming paper.

Acknowledgements

This study was carried out under GDRE ''Regular and Chaotic Hydrodynamics'' and supported by RFBR projects 10-05-00432-a, 10-05-00646-a, 09-01-92504/RUM1-2943-R0-09 from RFBR/CRDF, and by the Program ''The development of the scientific potential of higher school'' No. 2.1.1/554. Part of the study was carried out by MAS during his visit to LPO of UBO (Brest, France) in June–July 2008.

References

Baey, J.-M. and Carton, X., Vortex multipoles in two-layer rotating shallow-water flow. *J. Fluid Mech*. 2002, **460**, 151–175.

Carton, X., Hydrodynamical modelling of oceanic vortices. *Surveys Geophys*. 2001, **22**, 179–263.

Chérubin, L.M., Morel, Y. and Chassignet, E.P., Loop Current ring shedding: the formation of cyclones and the effect of topography. *J. Phys. Oceanogr*. 2006, **36**, 569–591.

Corréard, S.M. and Carton, X.J., Formation and stability of tripolar vortices in stratified geostrophic flows. *Il Nuov. Cim. C* 1999, **22**, 767–777.

Davis, R.E., Dolan, R. and Demme, G., Synoptic climatology of Atlantic coast North-Easter. *Int. J. Climatol*. 1993, **13**, 171–189.

Gluhovsky, A. and Klyatskin, V.I., On dynamics of flipover phenomena in simple hydrodynamic models. *Dokl. Earth Sci. Sec*. 1977, **237**, 18–20.

Gryanik, V.M., Dynamics of singular geostrophic vortices in a two-layer model of the atmosphere (ocean). *Izv. Atmos. Ocean. Phys*. 1983, **19**, 227–240.

Gryanik, V.M., Sokolovskiy, M.A. and Verron, J., Dynamics of heton-like vortices. *Regular Chaotic Dyn*. 2006, **11**, 383–434.

Hartman, D.L., Stationary planetary waves in the Southern Hemisphere. *J. Geophys. Res*. 1977, **82**, 4930–4934.

Hogg, N.G. and Stommel, H.M., The heton, an elementary interaction between discrete baroclinic geostrophic vortices, and its implications concerning eddy heat-flow. *Proc. R. Soc. Lond*. 1985a, **A 397**, 1–20.

Hogg, N.G. and Stommel, H.M., Hetonic explosions: the breakup and spread of warm pools as explained by baroclinic point vortices. *J. Atmos. Sci.* 1985b, **42**, 1465–1476.
Horton, C.W. and Baylor, K.J., Observations of cold-core Gulf Stream ring with an "explosive" elliptical instability. *J. Phys. Oceanogr*. 1991, **21**, 364–368.
Izrailsky, Yu.G., Koshel, K.V. and Stepanov, D.V., Determining the optimal frequency of perturbation the problem of chaotic transport of particles. *Dokl. Phys*. 2006, **51**, 219–222.
Izrailsky, Yu.G., Koshel, K.V. and Stepanov, D.V., Determination of optimal excitation frequency range in background flows. *Chaos*. 2008, **18**, 013107.
Kawakami, A. and Funakoshi, M., Chaos motion of fluid particles around a rotating elliptic vortex in a linear shear flow. *Fluid Dyn. Res*. 1999, **25**, 167–193.
Kennan, S.C. and Flament, P.J., Observations of a tropical instability vortex. *J. Phys. Oceanogr*. 2000, **30**, 2277–2301.
Kennelly, M.A., Evans, R.H. and Joyce, T.M., Small-scale cyclones on the periphery of Gulf Stream warm-core rings. *J. Geophys. Res*. 1985, **90**, 8845–8857.
Kizner, Z., Stability and transitions of hetonic quartets and baroclinic modons. *Phys. Fluids*. 2006, **18**, 056601.
Klyatskin, V.I., *Stochastic equations. Theory and its applications to the acoustics, fluid dynamics, and radiophysics*, Vol. 1–2, 2008. (Moscow: Fizmatlit).
Koshel, K.V. and Prants, S.V., Chaotic advection in the ocean. *Phys. Usp*. 2006, **49**, 1151–1178.
Koshel, K.V. and Prants, S.V., *Chaotic advection in ocean*, 2008. (Moscow-Izhevsk: Institute of Computer Sciences).
Koshel, K.V., Sokolovskiy, M.A. and Davies, P.A., Chaotic advection and nonlinear resonances in an oceanic flow above submerged obstacle. *Fluid Dyn. Res*. 2008, **40**, 695–736.
Lazutkin, V.F., Analytic integrals of a semistandard mapping, and separatrix splitting. *Algebra Anal*. 1989, **1**, 116–131.
McWilliams, J.C., The emergence of isolated, coherent vortices in turbulent flow. *J. Fluid Mech*. 1984, **146**, 1–43.
Morel, Y.G. and Carton, X.J., Multipolar vortices in two-dimensional incompressible flows. *J. Fluid Mech*. 1994, **267**, 23–51.
Nof, D., Generation of ringlets. *Tellus* 1993, **45A**, 299–310.
Perrot, X. and Carton, X., Point-vortex interaction in an oscillatory deformation field: Hamiltonian dynamics, harmonic resonance and transition to chaos. *Discrete Continuous Dyn. Syst. Ser. B*. 2009, **11**, 971–995.
Pingree, R.D. and Le Cann, B., Three anticyclonic Slope Water Oceanic eDDIES (SWODDIES) in the Southern Bay of Biscay in 1990. *Deep-Sea Res*. 1992, **39**, 1147–1175.
Richardson, P.L., Maillard, C. and Sanford, T.B., The physical structure and life history of cyclonic Gulf Stream ring Allen. *J. Geophys. Res*. 1979, **84**, 7727–7741.
Savchenko, V.G., Emery, W.J. and Vladimirov, O.A., A cyclonic eddy in the Antarctic Circumpolar Current south of Australia: results of Soviet-American observations aboard the R/V Professor Zubov. *J. Phys. Oceanogr*. 1978, **8**, 825–837.
Smeed, D.A., Baroclinic instability of three-layer flows: Part 2. Experiments with eddies. *J. Fluid Mech*. 1988, **194**, 233–259.
Sokolovskiy, M.A. and Verron, J., Finite-core hetons: Stability and interactions. *J. Fluid Mech*. 2000, **423**, 127–154.
Sokolovskiy, M.A. and Verron, J., Some properties of motion of $A+1$ vortices in a two-layer rotating fluid. *Russ. Sci. J. Nonlinear Dyn*. 2006, **2**, 27–54.
Solomon, T.H., Weeks, E.R. and Swinney, H.L., Chaotic advection in a two-dimensional flow: Lévy flights and anomalous diffusion. *Physica D* 1994, **76**, 70–84.
Sutyrin, G.G., Long-lived planetary vortices and their evolution: conservative intermediate geostrophic model. *Chaos*. 1994, **4**, 203–212.
Thivolle-Cazat, E., Sommeria, J. and Galmiche, M., Baroclinic instability of two-layer vortices in laboratory experiments. *J. Fluid Mech*. 2005, **544**, 69–97.
Zaslavsky, G.M., *The Physics of Chaos in Hamiltonian Systems*, 2nd ed., 2007. (London: Imperial College Press).